Geochemistry Geophysics Geosystems G3
AN ELECTRONIC JOURNAL OF THE EARTH SCIENCES
Published by AGU and the Geochemical Society

Article
Volume 2
June 13, 2001
Paper number 2000GC000129
ISSN: 1525-2027

Dynamical influences on the distribution and loading of SO_2 and sulfate over North America, the North Atlantic, and Europe in April 1987

Carmen M. Benkovitz, Mark A. Miller, and Stephen E. Schwartz
Brookhaven National Laboratory, Upton, New York 11973 (cmb@bnl.gov; miller@bnl.gov; ses@bnl.gov)

O-Ung Kwon
Korea Meteorological Administration, Seoul, Republic of Korea (oung@kma.go.kr)

[1] **Abstract:** The loading of tropospheric aerosols is highly variable spatially and temporally as a consequence of large spatial variability in sources, temporal variability in transport winds, and short residence times (days), and additionally for secondary sulfate, intermittent production associated with aqueous-phase reaction in clouds, and intermittent removal, mainly by precipitation. We have used a chemical transport and transformation model for atmospheric sulfur driven by observationally derived meteorological data to calculate the geographical distribution of sulfate and sulfur dioxide (SO_2) over North America, the North Atlantic, and Europe as a function of time for April 1987. We present the results of these calculations, mainly as animations showing the time dependence of the column burden (vertical integral of concentration) and of sulfate wet deposition, and interpret the temporal evolution in terms of the controlling meteorological phenomena as discerned from synoptic analyzes at 925 and 500 hPa. The analyzes show highly localized and episodic buildup and removal of sulfate and SO_2 and circulations under the influence of high- and low-pressure systems as well as instances of rapid meridional and zonal transport over distances of thousands of kilometers. Key meteorological phenomena giving rise to large amounts of sulfate include not only slow moving high-pressure systems, as previously recognized, but also low-pressure systems. Whether or not a given low-pressure system results in large sulfate loading depends strongly on its location relative to sources of sulfur species and of the water vapor that is required for formation of clouds and precipitation. We present a detailed analysis of the evolution of sulfate and SO_2 over the eastern North Atlantic April 3–8, 1987, under the influence of a cutoff low-pressure system during which sources in northern Europe continued to feed a system that repeatedly circulated over source regions. Animations such as these facilitate identification of episodes of large aerosol loading and relating these loadings to the controlling meteorological phenomena.

Keywords: Synoptic analysis; column burden; atmospheric model; cutoff low.

Index terms: Middle atmosphere — composition and chemistry; middle atmosphere — constituent transport and chemistry; troposphere — composition and chemistry; troposphere — constituent transport and chemistry.

Received December 8, 2000; **Revised** March 16, 2001; **Accepted** March 16, 2001; **Published** June 13, 2001.

Benkovitz, C. M., M. A. Miller, S. E. Schwartz, and O-Ung Kwon, 2001. Dynamical influences on the distribution and loading of SO_2 and sulfate over North America, the North Atlantic, and Europe in April 1987, *Geochem. Geophys. Geosyst.*, vol. 2, Paper number 2000GC000129 [13,830 words, 9 figures, 4 animations]. Published June 13, 2001.

1. Introduction

[2] Sulfate aerosol is of great interest because of its role in scattering solar radiation and modifying the reflectivity of clouds, with possible resultant influence on the Earth's radiation balance and climate [*Charlson et al.*, 1992, 1991; *Haywood et al.*, 1999; *Kiehl and Briegleb*, 1993; *Kiehl et al.*, 2000; *Mitchell et al.*, 1995; *Schimel et al.*, 1996; *Schwartz and Slingo*, 1996]. This material derives mainly from anthropogenic emissions of sulfur dioxide (SO_2) followed by oxidation in the atmosphere to form sulfate aerosol, which in turn is removed from the atmosphere mainly in precipitation. The characteristic times of the processes of formation and removal of sulfate and SO_2 are one to several days, so the geographical distribution of the material is confined principally to source regions, mainly industrialized regions of North America, Europe, and Asia, and to regions within a few days transport distance from these sources. At any given time the distributions of sulfate and SO_2 are dependent on the *synoptic-scale* meteorological fields over the past several days. (A glossary is presented in Appendix A). Because of the inherent variability in these meteorological quantities the distributions of sulfate and SO_2 exhibit substantial temporal variation as seen in time series of *mixing ratios* [*Benkovitz and Schwartz*, 1997, hereinafter B97; *Benkovitz et al.*, 1994, hereinafter B94; *Husain and Dutkiewicz*, 1990] or other measures of aerosol loading such as *optical depth* [*Wesely*, 1982].

[3] Because of the need to represent the radiative influence of sulfate in climate models, it is considered necessary to develop chemical transport and transformation models describing the loading and distribution of this material and to evaluate the performance of these models by comparison against observations. In view of the temporal variation in loadings that results from variability in the controlling synoptic-scale meteorology, it is virtually mandatory for the purpose of performing short-term comparisons with observations that the models be driven by observation-derived synoptic meteorological data. We have previously described a model that represents the distribution of sulfate and SO_2 for a domain covering North America, the North Atlantic, and Europe and have presented snapshots of the mixing ratio and *column burden* showing the large variation in the distributions of these quantities at different times as a consequence of day-to-day differences in the governing synoptic-scale meteorology (B94). This chemical transport and transformation model is driven by observation-derived synoptic meteorological data, specifically the output of the 6-hour operational forecast model of the European Centre for Medium Range Weather Forecasts (ECMWF). Simulations were performed for four periods of six weeks each in 1986–1987, and modeled mixing ratios were evaluated by comparison to an extensive set of observations at surface monitoring stations (B94, B97).

[4] To better display and interpret the temporal variation in the calculated loading of sulfate and SO_2 and relate these to the governing synoptic meteorology, we have prepared animations of the model output for a 32-day simulation in March and April 1987. These animations reveal temporal patterns that are not readily discerned in static displays. These animations show episodes of large loadings of sulfate and SO_2 that are a consequence of relations between the geographic distribution of sources and of the governing meteorological quantities that drive the transport and transformation model. Here we make use of these animations, together with animations of the controlling meteorological fields, to interpret the influence of synoptic-scale dynamics for particular episodes. Some of these episodes are associated with familiar *stagnation* conditions, such as the accumulation of trace species in

slow moving *anticyclones* [*Husar and Wilson*, 1993; *Husar et al.*, 1997; *Lyons*, 1980], also see Web page http://capita.wustl.edu/CAPITA/CapitaReports/BScatFMRelation/BSCATFM.html. The roles of other synoptic conditions associated with episodes of large sulfur loadings are less well documented, in particular, the accumulation of sulfate and SO_2 in *cutoff low-pressure systems*, a situation discussed in detail here.

[5] The organization of the rest of the paper is as follows. Section 2 describes the chemical transport and transformation model. Section 3 describes the meteorological regimes that occurred during the period of the simulation. Section 4 presents animations of the sulfate and SO_2 column burdens and relates the resulting patterns of these species to the meteorological conditions depicted in the synoptic animation. Section 5 presents isentropic analyzes of two cutoff lows that generated very different sulfate and SO_2 burdens, one over the western North Atlantic and the other over the eastern North Atlantic and examines the burdens of sulfate and SO_2 from individual source regions and formation processes and the vertical distributions of these species at an oceanic location under the influence of the cutoff low over the eastern North Atlantic. Section 6 presents our summary and conclusions, and section 7 discusses the implications of these findings.

2. Chemical Transport and Transformation Model

[6] The chemical transport and transformation model used in this study, the Global Chemistry Model driven by Observation-derived meteorological data (GChM-O), is a three-dimensional Eulerian transport and transformation model for SO_2, sulfate, and related species. The physical and chemical mechanisms used in the model have been previously described in B94 and B97 and are briefly described here. The model represents emissions of anthropogenic sulfate, SO_2 and of biogenic sulfur species, horizontal and vertical transport, gas-phase oxidation of SO_2 and dimethylsulfide (DMS), aqueous-phase oxidation of SO_2 by hydrogen peroxide (H_2O_2) and ozone (O_3) in precipitating liquid water clouds, and wet and dry deposition of SO_2, sulfate, and methanesulfonic acid (MSA). The sulfate and SO_2 variables are tagged according to source regions (North American anthropogenic, European anthropogenic, and biogenic), and, for sulfate, formation mechanism (*primary*; and *secondary* by *gas-phase* or *aqueous-phase* oxidation). *Seinfeld and Pandis* [1998] list the ocean, fossil fuel combustion and industry, plants and soils, and volcanos as the main sources of primary sulfate. In this work, only anthropogenic emissions of primary sulfate were included.

[7] The model is driven by observation-derived synoptic data obtained from the European Centre for Medium-Range Weather Forecasts (ECMWF), specifically the 6-hour *uninitialized analysis* [*ECMWF*, 1988], to allow comparison with observations at specific times and locations. The horizontal coordinates used are latitude and longitude with 1.125° resolution (~122 × 125 km at 12°N; 62.5 × 125 km at 60°N); the vertical coordinate is the ECMWF *eta (η) coordinate*, a system of terrain-following coordinates, with 15 levels between the surface and 100 hPa [*ECMWF Research Department*, 1991; *Simmons and Struffing*, 1981]. The model solves material balances based on the continuity equations with the application of *gradient transport assumptions* [*Bott*, 1989; *Easter*, 1993]; numerical approximations at any location are treated as mechanistically and dimensionally independent over short time steps according to an operator splitting technique [*Yanenko*, 1971]. Vertical transport occurs by eddy diffusion and by convective cloud mixing. The vertical eddy

diffusion coefficient was assumed to be 2.5 m^2 s^{-1} for the lowest model level (surface to ~65 m), 10 m^2 s^{-1} for model levels 2 to 4 (to ~2 km), and zero for all other model levels. The model time step is 0.5 hours for transport and 1 hour for cloud mixing, chemical reactions, and wet removal. The model output consists of the mixing ratio of all species at all model levels at 6-hour intervals. The mixing ratios were converted to concentrations and integrated vertically to give the column burden.

[8] The model domain (Figure 1) extends from circa 140°W to 62.5°E and 12.5°N to 81°N. Because of the restricted extent of the model domain, representative background values are assumed for mixing ratios of species that are advected into the model domain. These external contributions to loadings of sulfur species are relatively minor in regions within the model domain that are heavily influenced by anthropogenic emissions but represent an increasingly large contribution to the modeled loading of sulfur species near boundaries of the domain, especially in regions that are usually upwind of anthropogenic sources, that is toward the western side of the domain. The simulation was initiated with mixing ratios of sulfur and oxidant species in the model domain set to zero; the first two weeks of the simulation are considered model startup time and are not included in the analyzes.

2.1. Emissions

[9] Emissions of sulfur species in the model were taken to be representative of the March and April time frame circa 1985 (Figure 1) because estimates of the actual emissions for the specific simulation period do not exist. The model immediately distributes emissions uniformly throughout the volume of the grid cell into which the material is emitted. The development of the anthropogenic emission values is described by B97 and *Benkovitz et al.* [1996]; *primary sulfate* emissions (from fuel combustion, sulfuric acid production, etc.) were taken as 1.4% by mole of the total sulfur emissions for the United States and Canada and 5% for Europe. Estimates of emissions from ship traffic were not available for this simulation. Emissions from large point sources are introduced at the lowest three model levels (average heights above terrain 65, 230, and 540 m). The emissions exhibit considerable short-range variation even when aggregated to the 1.125° × 1.125° grid. Marine biogenic emissions of DMS [*Bates et al.*, 1992] were distributed to the 1° × 1° grid based on a global monthly gridded pigment concentrations derived from Coastal Zone Color Scanner (CZCS) images. Terrestrial biogenic emissions were calculated on a 1° × 1° grid using the methodology of Lamb [*Bates et al.*, 1992] and treated entirely as DMS. All biogenic emissions were then combined and converted to the 1.125° × 1.125° grid used by the model. Biogenic emissions in the model domain are ~5% of the anthropogenic emissions. Emissions from volcanoes, which were estimated to be ~0.6% of anthropogenic emissions, were not included in the simulations.

2.2. Dry Deposition

[10] Time- and location-dependent dry deposition of SO_2 and accumulation-mode particulate sulfate are represented in the model; dry deposition was calculated from surface resistance, atmospheric stability, surface wind speeds, and concentration of a species at the lowest model level [*Wesely*, 1989]. Dry deposition is an important removal mechanism for SO_2 but is minimal for sulfate, with an effective first-order removal rate of 5% per day at most.

2.3. Reactions and Oxidant Mixing Ratios

[11] Gas-phase oxidation of SO_2 and DMS is represented as pseudo first-order reactions using

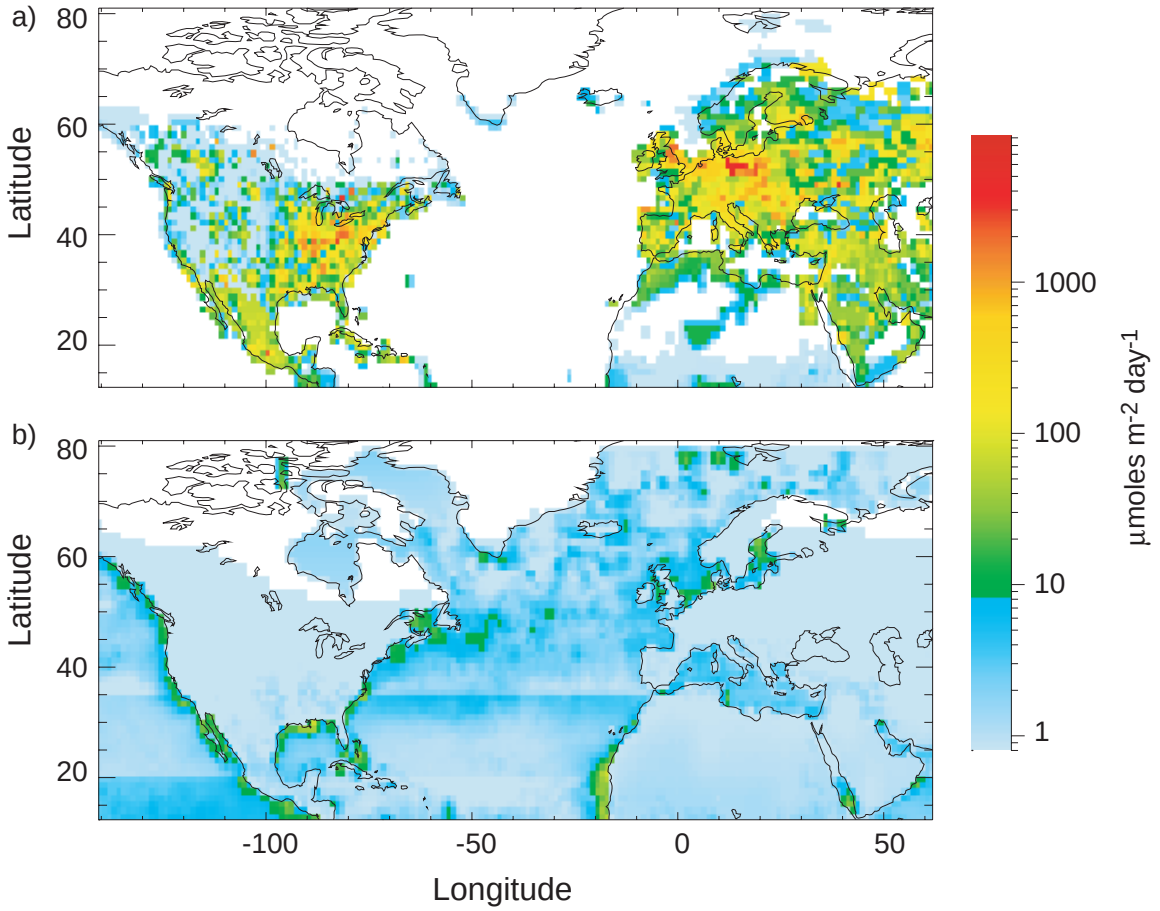

Figure 1. Geographic distribution of sulfur emission fluxes: (a) Anthropogenic emissions of sulfur (SO_2 plus primary sulfate) and (b) biogenic sulfur (DMS plus H_2S) emissions. The latitude band structure of the oceanic DMS emissions given by *Bates et al.* [1992] is still apparent after distribution proportional to coastal zone color scanner (CZCS) data and reallocation to the model grid, introducing discontinuities in these emissions. Note logarithmic scale; white denotes areas with no emissions.

diurnal-average OH mixing ratios. Climatological average OH mixing ratios every 5 days were obtained from the photochemical model calculations of *Spivakovsky et al.* [1990]. Aqueous-phase reactions were represented only in liquid precipitating clouds. Oxidation of SO_2 by hydrogen peroxide (H_2O_2) was limited by the lesser of either the SO_2 or the H_2O_2 mixing ratio. H_2O_2 was transported in the same way as the sulfur species, depleted by reaction with SO_2, and regenerated in the gas phase at a fixed rate (0.021 ppb h^{-1}) until a maximum mixing ratio (1.4 ppb) was reached. Aqueous-phase oxidation of SO_2 by ozone (O_3) was represented by a pseudo first-order reaction of gaseous SO_2 with a rate constant that takes into account an assumed O_3 mixing ratio of 37.5 ppb, O_3 solubility, the solubility and dissociation of gaseous SO_2, and the cloud liquid water content. Cloud water pH, governing the rate of SO_2 oxidation by O_3, was taken as 4.5.

3. Meteorological Considerations

[12] During the spring season, rapid fluctuations occur between different types of synoptic

regimes such as high-amplitude *meridional meanders*, *cutoff lows*, and *zonal flow*. The wide range of synoptic regimes aids in understanding the influence of various synoptic features on the spatial and temporal variation of the transport and loading of trace species, here specifically mixing ratio and column burden of sulfate and SO_2. The connection between evolving meteorological flow features and the sulfate and SO_2 distributions is examined using meteorological analyzes from two pressure levels in the troposphere, 925 and 500 hPa. Plots of the 925 and 500 hPa synoptic analyzes were developed every 6 hours, and animations were generated from these plots. Gridded data from the National Center for Atmospheric Research (NCAR) Reanalysis Project [*Kalnay et al.*, 1996] were used in the synoptic analyzes. As noted above, the sulfate and SO_2 simulations were driven by the ECMWF uninitialized analyzes. The same underlying synoptic data are used in both analyzes, albeit with inevitable differences between the meteorological fields in the two analyzes and subtle differences in the hemispheric height (wind) fields resulting from differences in the objective analysis schemes. The similarity of the meteorological fields suggests that these differences do not significantly impact the interpretation of the governing transport processes.

[13] Synoptic-scale flow is strongly influenced by the *jet stream*, which is determined by the horizontal gradients of the height of constant pressure surfaces. Figure 2 shows an example of the heights above mean sea level that correspond to pressures of 500 and 925 hPa for April 15 1800 UT. Representative average heights above sea level are 5420 m at 500 hPa and 780 m at 925 hPa. Positive and negative height anomalies on the constant pressure surfaces, corresponding to high- and low-pressure systems respectively, give rise to clockwise (anticyclonic) and counterclockwise (cyclonic) wind circulations. To a good approximation, the wind speed at a given point on the constant pressure surface is directly proportional to the magnitude of the height gradient at that point. The wind direction is roughly parallel to the contours, with lower heights to the left of the wind vector in the Northern Hemisphere, as illustrated in Figure 3. In Figure 2 the main axis of the jet stream roughly parallels the 5400-m height contour. Associated with meridional meanders in the jet axis like the one over the eastern United States, there are regions of generally west-to-east height gradients that result in zonal flow. Examples of zonal flows are indicated in Figure 2.

[14] Horizontal transport of material by the circulations at these two pressure levels is quite different, as indicated by the varying configuration of the height gradients over specified points in the flow. Vertical transport of material in cyclones is characterized by large-scale motion away from the surface and abundant precipitation. Conversely, vertical transport of material in anticyclones is characterized by downward motion, absence of precipitation, and strong low-level inversions. Large sulfate column burdens near the surface are commonly associated with anticyclones and resultant stagnation episodes, but the present model results suggest large sulfate column burdens may also occur in association with the decaying stages of certain cyclones, depending on their location relative to emission sources, as discussed later.

[15] Systems with circulations extending through the depth of the troposphere are capable of accumulating material within their region of influence. Significant events of the anticyclonic or cyclonic type are defined by at least one "closed-contour" at the 500 hPa level, so the climatology of 500 hPa cyclones and anticyclones is an important factor in determining the distribution of material over the hemisphere. The terminology "cutoff low" is typi-

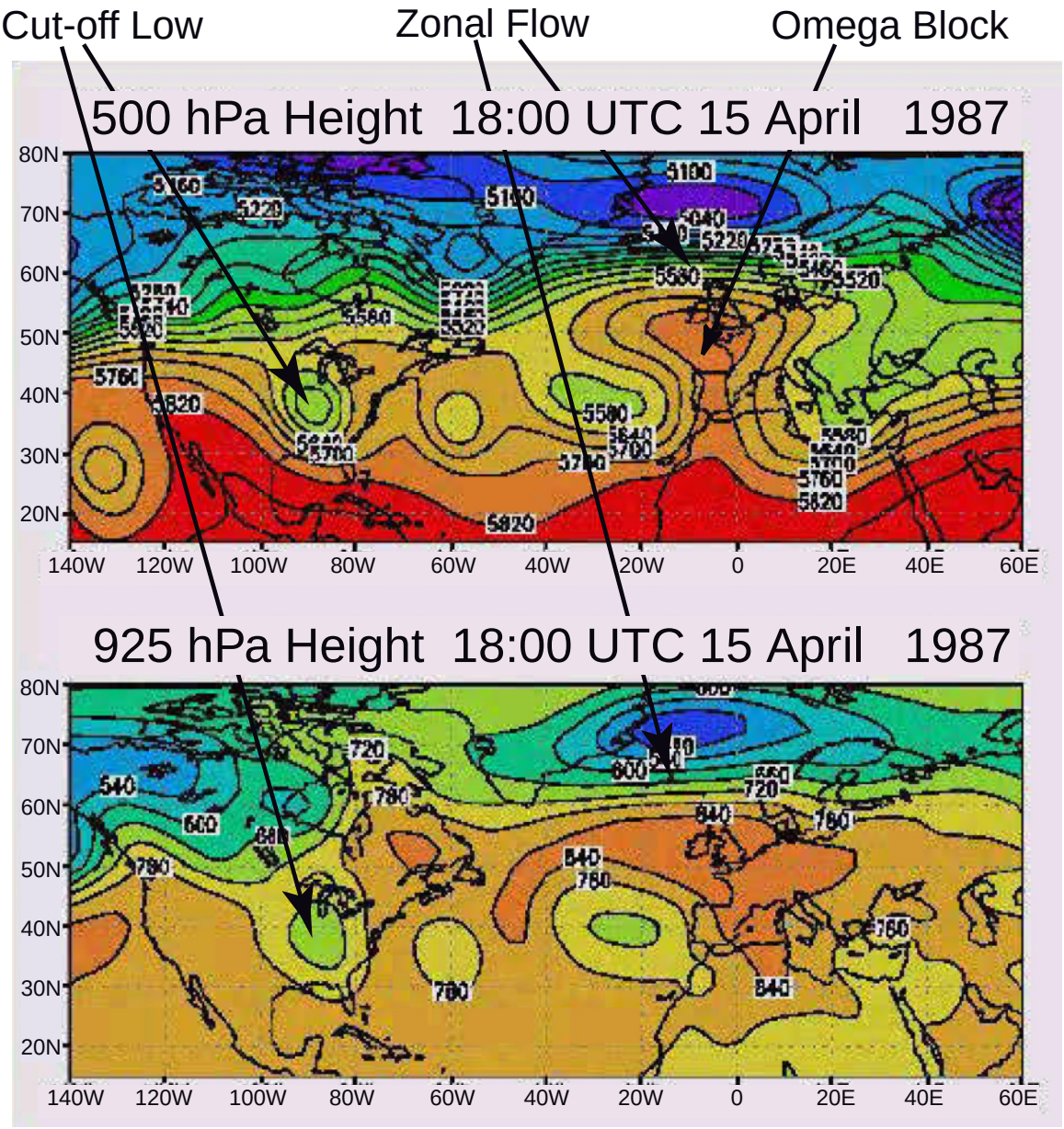

Figure 2. Synoptic analysis at the 500 and 925 hPa surfaces for April 15 1800 UT. The arrows point to areas of zonal flows and a cutoff low in the 500 and 925 hPa panels and to an omega block in the 500 hPa panel. Cooler colors (blue, green) represent lower values of the height of the surface, hotter colors (yellow, red) represent higher values of this height.

cally interchanged with "500 hPa cyclone" because no formal definition distinguishing them has been established. The climatology of anticyclones and cutoff lows at 500 hPa has been examined by *Parker et al.* [1989] and the climatology of cutoff lows at 200 hPa by *Kentarchos and Davies* [1998]. These studies show that overall, 500 hPa cyclones and

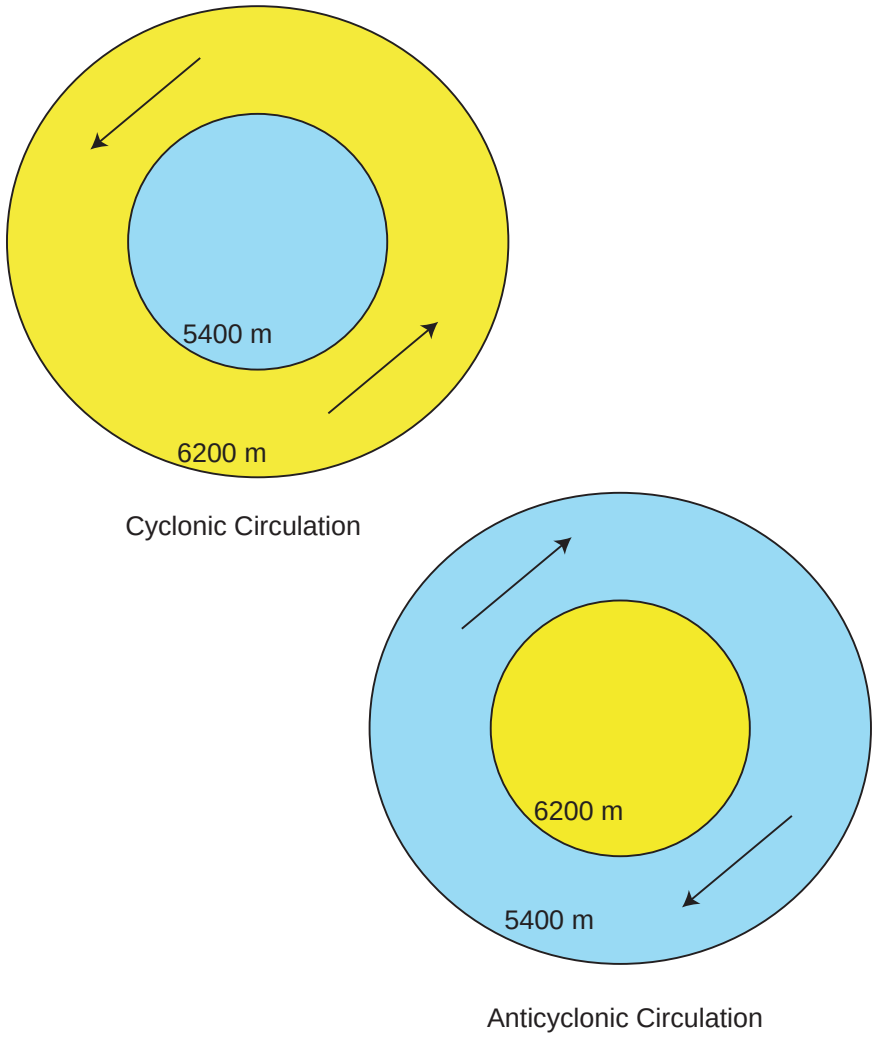

Figure 3. Illustration of wind flows around anticyclonic and cyclonic circulations. In the Northern Hemisphere, low height (low pressure, cool color) contour is always to the left of the wind vector, cyclonic circulations are counterclockwise, and anticyclonic circulations are clockwise.

anticyclones are infrequent events, observed less than 10% of the time at any given location. Cyclones at 500 hPa are more common than anticyclones. Geographically, 500 hPa cyclones are found primarily at middle and high latitudes, whereas 500 hPa anticyclones are found primarily at subtropical latitudes. The frequency of 500 hPa cyclones over the northern oceans increases during the summer, and the frequency of 500 hPa anticyclones increases over the subtropics, although there are departures from these geographic generalities, which include a southward extension of relatively higher 500 hPa cyclone frequency observed near southwestern Europe throughout the year. These studies also show that there are significant year-to-year differences in the frequency of cutoff lows.

[16] During the simulation period examined here an intense cutoff low system developed over the eastern North Atlantic on April 3–8,

manifested by concentric height contours surrounding a height minimum on the 500 hPa analysis. The circulation of this system was completely separated from the jet stream, and it controlled the transport, removal, and accumulation of material over the region of influence. The internal circulation around a cutoff low prevents ventilation by air masses from other locations; thus there is little opportunity for material to be dispersed over regions outside the influence of the cutoff low. When a synoptic system reaches occlusion, which is the decaying stage of any cyclone, the surface circulation and upper airflows become vertically aligned. Therefore occluded surface systems are often associated with cutoff lows at 500 hPa. Under some circumstances, there is little ventilation of atmospheric tracers in cutoff lows because material is not moved vertically and subsequently transported out of the system by winds at different levels. Within the core of a cutoff low, material may be transported vertically through three-dimensional motions and convection, so accumulation is possible at all levels.

[17] A useful way to follow the three-dimensional transport in synoptic-scale circulations is by means of *isentropic analysis* [*Namais*, 1938, 1939]. This analysis can reveal regions of *slantwise ascent* or descent that take place over synoptic spatial (1000 km^2) and temporal (days) scales and are so named to differentiate them from vertical motions on smaller length scales and on shorter timescales, such as those associated with individual clouds. Slantwise motions are organized features of midlatitude cyclones that can transport material over long distances with simultaneous ascent or descent.

[18] We combine isentropic analyzes with examination of modeled mixing ratios to depict the development of the three-dimensional distribution of the modeled species. Isentropic surfaces at *equivalent potential temperatures* of 295°K, 300°K, 305°K, 310°K, and 320°K are presented in Figure 4 for April 1 0000 UT. The lower the temperature of the isentropic surface, the lower it is in the *troposphere*; the 320°K surface represents conditions in the upper troposphere, whereas that at 295°K represents the lower troposphere. Isentropic analysis is most useful at higher levels of the troposphere where isentropic surfaces are not interrupted by intercepting the ground; it is less useful at lower tropospheric levels where the surfaces intercept the ground in the tropics and in mountainous areas, as indicated by the gray areas on the 295°K, 300°K, and to a lesser extent the 305°K isentropic surfaces.

4. Animations of the Meteorological Analysis and the Sulfur Column Burdens

4.1. Introduction

[19] Plots of the column burden of sulfate and SO_2 and of the wet deposition of sulfate were used to generate the animations that provide an overview of the temporal evolution of the atmospheric loading of these species. In this section we present these animations and the animation of the synoptic analysis at the 925 and 500 hPa surfaces for the period April 1 to 30, 1987. The date and time are shown in the lower left of the column burden panel in the following format: YY MM DD HH corresponding to year, month, day, and hour (UT); for the synoptic analysis the date and time are shown in the title of each panel.

[20] Animations are available at http://www.g-cubed.org/publicationsfinal/articles/2000GC000129/a2000GC000129.html. To display the animations, click on the links for synoptic animation (Animation 1), for sulfate column burden (Animation 2), SO_2 column burden (Animation 3), and sulfate wet deposition (Animation 4), respectively. The anima-

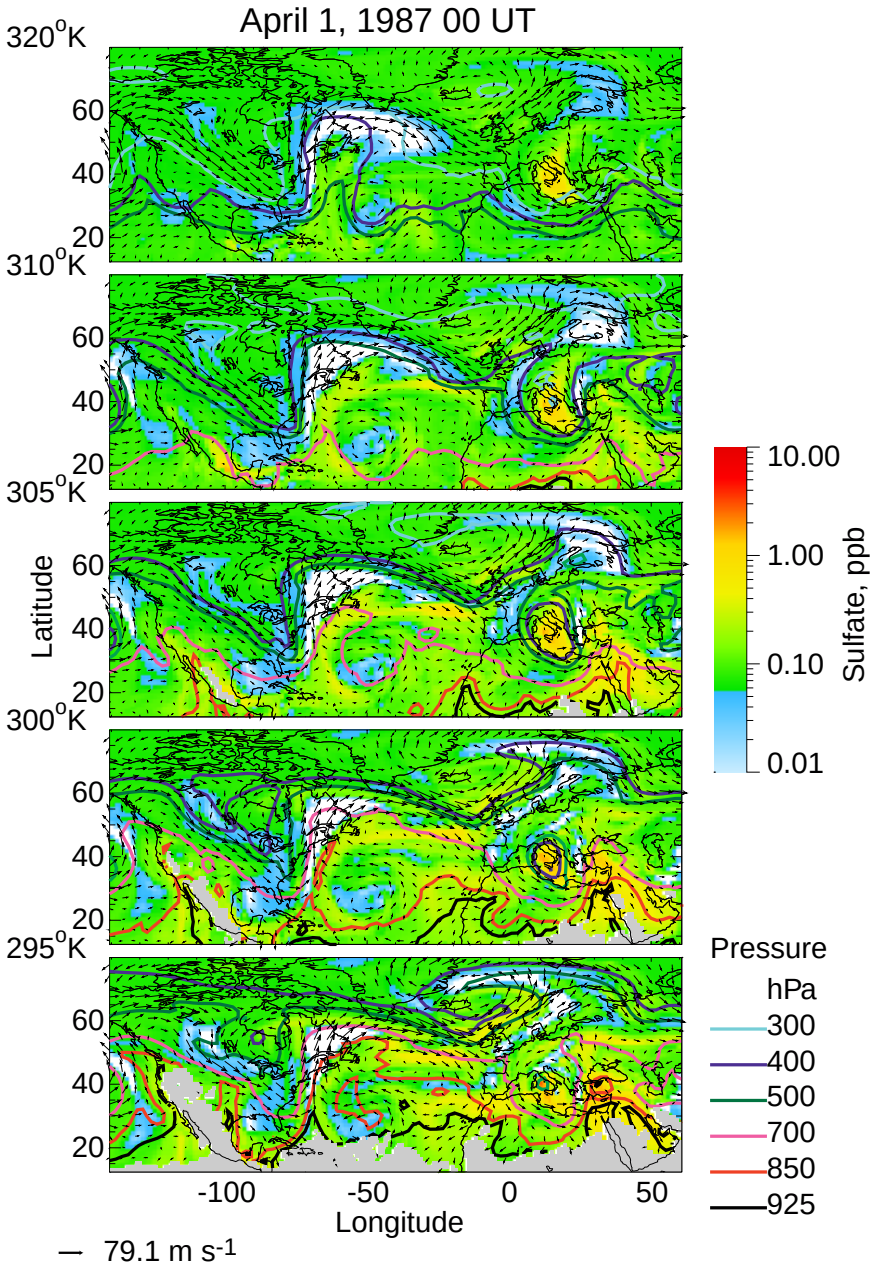

Figure 4. Isentropic analysis for April 1 0000 UT at the 295°K, 300°K, 305°K, 310°K, and 320°K surfaces. The potential temperature is constant at all points on each chart, and the contours represent constant barometric pressures. The colors denote the sulfate mixing ratio on the isentropic surface. Gray areas denote the intersection of isentropic surfaces with the ground; white areas denote regions where the sulfate mixing ratio was <0.01 ppb. Arrows indicate wind velocity; scale arrow indicates maximum velocity.

tions are set up to be viewed at 4 frames per second, corresponding to one model day per second. Examination of these animations shows the substantial temporal variation in the loading of both species in addition to the spatial variation that is manifested in the individual frames. The animations also illustrate the transport of these species under the influence of the synoptic flow. Attention is called to the logarithmic scale used to display the wide dynamic range represented in both animations, 3 orders of magnitude for sulfate and 4 orders of magnitude for SO_2, and to the fact that the maxima in the ranges are scaled to the overall maxima of the column burdens, a factor of 4 higher for SO_2 than for sulfate.

[21] Some observations about the animations may be noted:

1. Both sulfate and SO_2 exhibit patterns that are driven by synoptic-scale atmospheric circulations. SO_2 tends to exhibit plume-like behavior that is more continuously traceable back to source regions such as the Great Lakes area and northern Germany than sulfate. This reflects the continuous nature of SO_2 sources and sinks versus the episodic nature of the aqueous-phase formation of sulfate and its removal associated mainly with precipitation events. Examples of the episodic nature of sulfate formation can be seen in the abrupt increase on April 6 from 0000 to 0600 UT near Kiev; on April 10 from 0600 to 1200 UT in the Illinois-Indiana area; and on April 15 from 0600 UT to 1200 UT again in the Illinois-Indiana area.
2. Long-range transport (thousands of kilometers) is readily discernable for both sulfate and SO_2, in some instances extending across the entire North Atlantic from North America to Europe. Attention is called to an instance of large column burden of SO_2 transported from the Great Lakes area (March 29 1200 UT) to the Iberian Peninsula (April 1 1200 UT) and to large column burden of sulfate transported from New England (April 23 1800 UT) to the Canary Islands (April 25 1800 UT). Note that a sulfate column burden of 300 μmol m^{-2} would, for a mass extinction efficiency of 8.5 m^2 g^{-1} at 500 nm [*Charlson et al.*, 1992], yield an optical depth of 0.25.
3. Wet deposition events can lead to efficient removal of sulfate as manifested by the colocation of wet deposition and reductions in sulfate column burden, for example, on April 1 1800 UT the colocation of wet deposition over the Great Lakes, New England, southwest of Ireland, North Sea and western France, and north of Scandinavia. The efficient removal of sulfate in precipitation is often manifested by the abrupt appearance of regions of extremely low sulfate column burden indicated by localized green or even blue regions in the animation, for example, from March 29 1800 UT to March 30 0000 UT in the southeast United States and from April 12 0000 UT to April 12 0600 UT in the mid North Atlantic.
4. A particularly striking event occurred on April 3–8 during which substantial amounts of sulfate and SO_2 were advected from the European continent to the North Atlantic west of France and the Iberian peninsula. This episode and several others are discussed in subsequent sections.

4.2. Narration

[22] Set the sulfur animations to April 1 0000 UT, which is the beginning time of the synoptic analysis. On April 1 0000 UT the synoptic flow off the northeast coast of the United States into the Canadian Maritimes was southwesterly at both 500 and 925 hPa. The sulfur animations show well-defined minima in sulfate and SO_2 associated with this southwesterly flow, which can be readily discerned by stepping the sulfate

and SO_2 animations from March 31 0000 UT to April 1 0000 UT. This region of low sulfur corresponds to an instance of a well-developed *warm conveyor belt*, a cloud and precipitation system in which maritime tropical air is *advected* northward and up slope along the edge of a colder air mass. The superposition of flow features at many levels leads to the organized transport of parcels to a higher level in the atmosphere. The cloud and precipitation system associated with a warm conveyor belt on satellite images is commonly termed a *baroclinic leaf*, a system of saturated air parcels that produces clouds over a wide area and that may produce copious amounts of precipitation. Clouds associated with a baroclinic leaf enhance conversion of SO_2 to sulfate but also remove sulfate in precipitation. As a result, their impact on the sulfate burden can range from a large source to a large sink, depending on the relative balance of formation by in-cloud reaction and removal in precipitation.

[23] The minimum in the sulfate column burden corresponds to the three-dimensional parcel trajectories associated with the baroclinic leaf structure and to regions of low sulfate mixing ratio indicated by the white areas in the isentropic surfaces on April 1 0000 UT (Figure 4). Wind vectors off the east coast of the United States show southerly flow, with parcels moving from the 800 hPa isobar off the coast of Florida to the 600 hPa isobar over the Canadian maritime provinces, indicating widespread slantwise ascent. Assuming an average horizontal velocity of 15 m s^{-1} (a typical value for these conditions), for a 1000 km south to north transport the corresponding vertical velocity is approximately -3×10^{-3} hPa s^{-1} (-3 cm s^{-1}, a moderate rate of ascent). A synoptic-scale vertical velocity of this magnitude indicates slow, methodic ascent that will give rise to widespread precipitation typical of midlatitude cyclones and lead to efficient removal of any sulfate present. Note also that the flow turns sharply west-northwest off the coast of eastern Labrador, so precipitating air parcels moving upward and to the northeast, off the northeast coast of the United States, continue to ascend and may eventually arrive at 400 hPa. At that level the flow is diverted toward the southeast with accompanying precipitation and consequent removal of sulfate.

[24] An example of low sulfur burden in a maritime cutoff low is seen at 50°W and 30°N. The synoptic charts reveal a well-defined cutoff low at 500 hPa that was vertically aligned with a weak low-pressure center at 925 hPa, a classic signature. The circulations associated with this cutoff low may be discerned by stepping the sulfate and SO_2 animations from March 31 1800 UT to April 1 1800 UT. There was little SO_2 because the cutoff low was far removed from local sources, the transit time allowed for conversion to sulfate, and the system was isolated from input by advection. Precipitation had removed sulfate in this system, despite a precipitation rate that was not so large as in the warm-conveyor belt described above. In this circumstance,the cutoff low acted as a sink for sulfur.

[25] The synoptic analysis for April 1 0000 UT shows a second cutoff low, situated over Italy. Meteorologically, this disturbance was dissimilar to the baroclinic leaf off the Labrador coast but similar to the cutoff low in the central Atlantic. In contrast to the system in the central Atlantic, the cutoff low over Italy was located over a continental region with SO_2 sources. Note the circulation of sulfate and SO_2 in the low between April 1 0000 UT and April 2 0600 UT. The showery precipitation was less intense because of less moisture availability, so SO_2 from the local sources accumulated and was oxidized to sulfate. The result was that these two cutoff lows, not dissimilar in structure, had markedly different impacts on the atmospheric sulfur burden because of their geographic loca-

tion. Depending on their dynamic structure, cutoff lows may be able to sustain large sulfur column burden through accumulation, as if the storm were a large reaction vessel, with sulfur being continually added but removed at a slower rate. Whether or not this occurs depends on the location of the cutoff low relative to emission and moisture sources.

[26] Advancing the three animations to April 3 0000 UT, the 500 hPa surface shows the development of a high-amplitude *trough* off western Europe with an associated strong surface storm indicated in the 925 hPa panel. At this time, there was a broad area with large SO_2 burden that extended through northern Europe across the North Sea and into the Atlantic just to the north of the United Kingdom. The corresponding sulfate burden was considerably lower, most likely owing to the lack of aqueous-phase oxidation caused by the entrainment of dry air from the Middle East deserts into the low centered south of the United Kingdom. The synoptic analysis animation from April 3–5 0000 UT shows the evolution of this high-amplitude trough into an intense cutoff low. During this period the air mass from over the European continent was drawn into the developing cutoff low, as indicated by the large SO_2 burden, and the dry air was eventually moistened as it wrapped around the system, producing sulfate column burden of several hundred $\mu mol\ m^{-2}$ south of the low by April 5 0000 UT. Large values of the sulfate column burden persisted in the region for more than 72 hours, as manifested by advancing both sulfur animations to April 6 1200 UT.

[27] In addition to the maximum in the sulfate column burden associated with the cutoff low over the coast of France and Portugal on April 6 1200 UT, there was a region to the east of this feature, centered at $\sim 50^\circ$N and 40°E, that exhibited localized sulfate burdens in excess of 300 $\mu mol\ m^{-2}$ and SO_2 burdens in excess of 600 $\mu mol\ m^{-2}$. The nature of this second maximum over the interior of Europe is best explained by examining both the sulfate and the SO_2 animations. The SO_2 animation (Animation 3) shows a well-defined band of large SO_2 column burden that extends from Ireland to just north of the Black Sea. This band is associated with *confluence* in the upper level flow, indicated by a tightening of the pressure gradient along this flow in the synoptic animation. In this confluence zone, SO_2 is transported to the northeast from sources in Spain and southern Europe and is transported to the southeast from sources in Scandinavia; in addition, there are numerous SO_2 sources in vicinity of the band itself. It is this configuration of SO_2 that modulates the corresponding sulfate column burdens; the sulfate animation (Animation 2) for this period shows that its geographic distribution is dictated by the conversion time from SO_2 to sulfate, which because of the lack of moisture is dominated by the slow gas-phase conversion mechanism.

[28] The synoptic animation (Animation 1) shows that conditions over the region that experiences large sulfate burden were slowly changing from April 8 1200 UT through April 10 1200 UT. The ridge at 500 hPa at $\sim 0^\circ$ and extending to the northeast slowly progressed toward the east and was replaced by a trough beginning in the vicinity of 30°N also at 0°. At 925 hPa the progression of events is best captured by observing the southeastward expansion of the 720 m contour surrounding an area of low pressure to the northwest. Thus the 925 hPa ridge that contained the large SO_2 column burden was slowly replaced by a trough that was associated with surface convergence of material and the formation of clouds. The clouds associated with the encroaching trough formed in an area with large column burden of SO_2 that was then oxidized to sulfate.

[29] On April 9 1200 UT an *"omega (Ω)" blocking pattern* had formed at 500 hPa over Scandinavia; this stable flow configuration impedes the development and advection of synoptic-scale storms for periods of typically 1 week. The core of this block is represented on the 500 hPa analysis by the green-colored region between 5400 m and 5460 m that outlines the omega-shaped (Ω) 5400 m contour; the 5460 m contour south of Scandinavia marks the southern boundary of the block. Overall, ridging conditions existed in the 500 hPa height field at this time from 20°N to 50°N from the 0° meridian to the northeast. Subsidence, high surface pressure, and stable conditions in the lower troposphere dominated the flow east of the axis of this extended ridge, and the 925 hPa flow showed little height gradient in the core of the omega block and south to 20°N. These features accounted for persistent large SO_2 column burden over an extended area; the largest SO_2 column burden was in the core of the block and the largest sulfate column burden along the ridge line.

[30] Advancing the synoptic animation from April 9 1200 UT through April 11 1200 UT shows that the omega block initially over Scandinavia persisted and migrated slowly toward the east, but the transient ridge found at 500 hPa south of the omega block on April 9 1200 UT was replaced by a trough. In addition, low heights at 925 hPa developed over the area in association with a weak surface low-pressure system. The complete progression of events for the 3 day period began with accumulation of SO_2 in the stagnant air mass beneath the ridge extending from the base of the Scandinavian omega block to the Mediterranean and continued with the slow replacement of the ridge with a weak trough over the region that enhanced surface convergence, formed clouds, and oxidized SO_2 to sulfate. As this system moved to the east, a weak low-pressure system slowly developed which enhanced precipitation and depleted sulfate.

[31] The importance of proximity to local sources is reinforced by noting that on April 11 1200 UT the pronounced ridge at 500 hPa in the central and eastern Atlantic, and its associated strong anticyclone at 925 hPa, were not characterized by large SO_2 column burden despite apparently favorable meteorological conditions for accumulation. A much weaker ridge at 500 hPa over the eastern Great Lakes, a region characterized by important sources of SO_2, exhibited SO_2 column burden that were at least 3 orders of magnitude larger than over the western Atlantic. On April 11 1200 UT the largest column burdens were in the vicinity of similarly shaped ridges in northern Poland and Sweden, and in the eastern Great Lakes, both located close to major source regions, but not over the central and western Atlantic where there was a stronger anticyclone but no major sulfur sources.

[32] A circumstance in which an interaction between two synoptic disturbances conspired to produce a local maximum in the sulfate burden is shown by advancing all animations to April 12 1200 UT. At this time a significant *blocking ridge* was present in the upper midwestern United States, and an associated strong anticyclone at 925 hPa was centered over Hudson's Bay beneath the eastern half of the blocking ridge. Coexisting with this upper level ridge was a weak trough on its southern edge over Lake Michigan. This upper level trough was characterized by relatively weak height gradients at 925 hPa, absence of any organized cyclone, and quite large sulfate column burden. There were several dynamic reasons why the column burden was so large in this region. The weak trough aloft produced weak surface convergence of vapor, sulfur, and clouds but little or no precipitation. This convergence was superimposed on an air mass

that was previously stable and had weak winds and a strong inversion associated with its position along the southern edge of the strong anticyclone to the north. These conditions led to large sulfate column burden in this region prior to the appearance of the weak trough, as shown by rewinding the sulfate animation (Animation 2) a few frames and again advancing; note the lazy clockwise circulation. Hence a reason for the large sulfate column burden over Lake Michigan was the superposition of weak convergence on a region of preexisting large sulfate burden; this convergence brought the existing sulfate into the core of the anticyclone. Conceptually, this situation is similar to *frontogenesis* in which the horizontal gradient of a passive scalar (temperature in fronts) is strengthened owing to a converging wind field.

[33] Advancing all animations to April 15 0000 UT shows a newly formed omega block at 500 hPa over western Europe, centered south of Ireland. The associated strong anticyclone at 925 hPa gave rise to the largest sulfate and SO_2 column burden in the model domain. In contrast, a pronounced SO_2 maximum was observed over the midwestern United States associated with a well-defined cutoff low, but the sulfate burden in this system was markedly lower than that observed in association with the European anticyclone. Examination of the evolution of these synoptic features affords an opportunity to compare and contrast the various mechanisms that are responsible for sulfate distributions. Advancing all animations to April 16 0000 UT shows that both the omega block over western Europe and the cutoff low over the Ohio River valley were slow moving weather systems. During the 48 hours between April 14 0000 UT and April 16 0000 UT the cutoff low over the eastern United States was drifting over a region rich in SO_2 sources so both the sulfate and the SO_2 column burdens increased. From April 16 0000 UT until April 20 0000 UT, little changed with respect to these two synoptic patterns or the associated sulfate column burden, except that the cutoff low drifted slowly off the East Coast of the United States and thus away from the SO_2 sources. When this system moved offshore, it was deprived of SO_2 sources and acquired access to moisture, thus generating clouds and precipitation, which increased the oxidation rate of SO_2 to sulfate and concurrently removed the sulfate. By April 21 0000 UT the column burden of sulfate associated with the cutoff low decreased substantially (by 200–400 μmol^{-2}). In contrast, the column burden of both sulfate and SO_2 associated with the omega block in western Europe remained large, drifted over the eastern Mediterranean, and covered a larger region.

[34] In April 1987, omega blocks at 500 hPa, which occurred intermittently from the second through the fourth weeks of the month, were associated with large sulfur column burden, although the burden waxed and waned as the block temporarily disappeared and then reappeared. Advancing the animations to April 22 0000 UT shows the formation of another omega blocking pattern over western Europe, extending into Scandinavia. Advancing the animations to April 24 0000 UT shows that the ridge in this region continued to exist despite losing its characteristic omega shape; by April 28 0000 UT the omega block returned. If these blocks recur frequently over regions that have important emission sources the chemistry and radiation climatology of the region can be substantially impacted.

[35] A large ridge formed in Southern California by April 28 0000 UT, accompanied by a modest, widespread increase in sulfate column burden rather than a pronounced, highly concentrated increase. Significantly lower emission fluxes of sulfur were present over the western United States than the eastern United States or western Europe as shown in Figure 1. There-

fore, in this region the impact of weather systems, such as cutoff lows, that repetitively circulate the same air mass will not be so extreme as over the eastern United States or western Europe.

5. Cutoff Lows Over the Eastern and Western Atlantic, April 3–8

[36] This section uses isentropic analysis and the identification of sulfate by source region and production mechanism to examine why a cutoff low on April 3–8 along the eastern margin of the Atlantic generated large quantities of sulfate, whereas a cutoff low on the same dates along the western margin of the Atlantic did not. The meteorological dynamics of the two systems were similar, yet the sulfate mixing ratios on all isentropic surfaces were markedly different. There were regions around the eastern Atlantic system where the sulfate mixing ratio exceeded 1 nmol/mol air (1 ppb), whereas the mixing ratio around the western Atlantic system was an order of magnitude lower.

[37] Isentropic analysis for April 3–5 at several different equivalent potential temperatures (Figures 5, 6, and 7) relates the mixing ratio of sulfate and SO_2 to synoptic-scale air parcel trajectories. It also relates clouds and precipitation along a parcel three-dimensional trajectory that encounters sulfur sources to sulfur transformation and sinks.

[38] In general, before low-pressure systems reach the occluded (or cutoff low) stage, they are characterized by a synoptic-scale region of slantwise ascent on the eastern side of the 500 hPa trough; the likelihood of the parcels undergoing slantwise ascent to eventually produce precipitation depends on the availability of surface moisture at the start of the ascent. Prior to the formation of the cutoff lows, the low-pressure system over the western Atlantic had lifted moisture-laden parcels originating over the warm Gulf of Mexico and the Atlantic Ocean. This gentle upward transport of parcels is indicated by wind vectors crossing isobars in the 305°K isentropic surface of Figure 5. The wind vectors show that parcels undergoing isentropic (adiabatic) ascent are moving through progressively lower-pressure surfaces, which are increasingly higher in the troposphere, as they move from south to north. This upward motion represents a slow cooling of relatively moist parcels (actual temperature not potential temperature) that generated precipitation which removed sulfate (see Animation 4 for April 3 0000 UT to April 4 0000 UT), so the sulfate column burden was small. In contrast, the low-pressure system over the eastern Atlantic had transported relatively dry parcels originating from cold land surfaces over continental Europe upward in the atmosphere. These drier parcels must be moved farther upward in the troposphere to experience saturation and precipitation, so there was little opportunity for precipitation and sulfate removal.

[39] On April 4 0000 UT (Figure 6) the cutoff low along the eastern Atlantic exhibited concentric circulation on the 295°K, 300°K, and 305°K isentropic surfaces, with little slantwise transport into or out of the core of the disturbance. This was an indication that the disturbance was entering the final phase of its life cycle, an observation consistent with the lack of precipitation production and its vertical alignment on the synoptic animation. On April 5 0000 UT (Figure 7) both lows exhibited concentric circulations in almost all isentropic surfaces, but the system along the western Atlantic continued to generate precipitation (compare the sulfate column burden and the sulfate wet deposition for this date) so its associated sulfate column burden was still small. The cutoff low along the eastern Atlantic was much larger, and it continuously recircu-

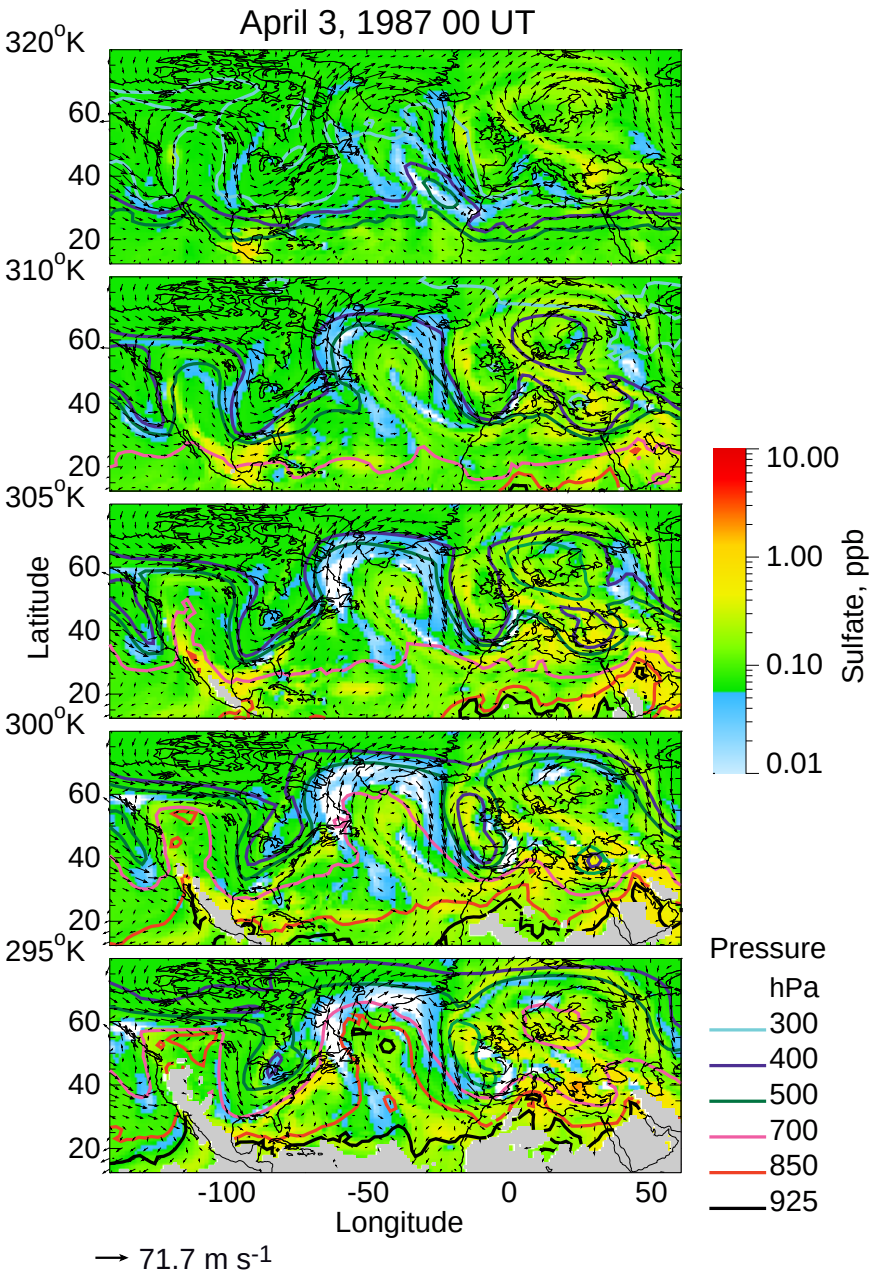

Figure 5. Isentropic analysis for April 3 0000 UT. As in Figure 4.

lated the same air mass over western European sulfur sources, which accounts for the increase of the sulfate column burden during the lifetime of this low. The vertical diffusion from surface sources occurred in the form of SO_2 transport and subsequent conversion to sulfate. The sulfate column burden generated by this cutoff low was large, it extended over a wide area, and it remained in the atmosphere for a relatively long time.

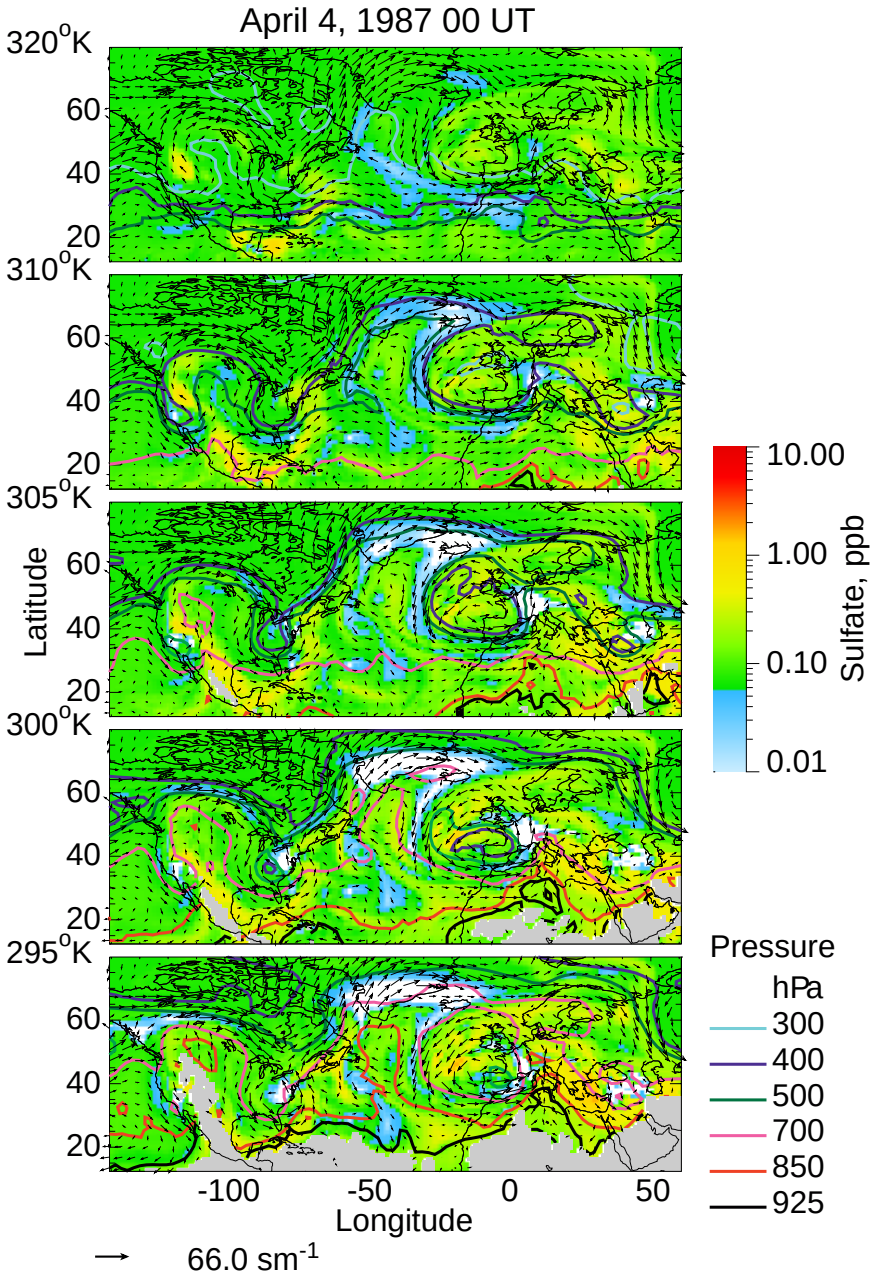

Figure 6. Isentropic analysis for April 4 0000 UT. As in Figure 4.

[40] To gain further insight into the dynamical influences of meteorology on column burdens and vertical profiles of the concentrations of sulfate and SO_2 during the April 3–8 cutoff low over the eastern Atlantic, we examine the sulfate and SO_2 by source region and formation mechanism. On April 5 0600 UT (Figure 8) the region of large SO_2 column burden was located along the northern border of the cutoff low, where the pressure gradients were sharp (height

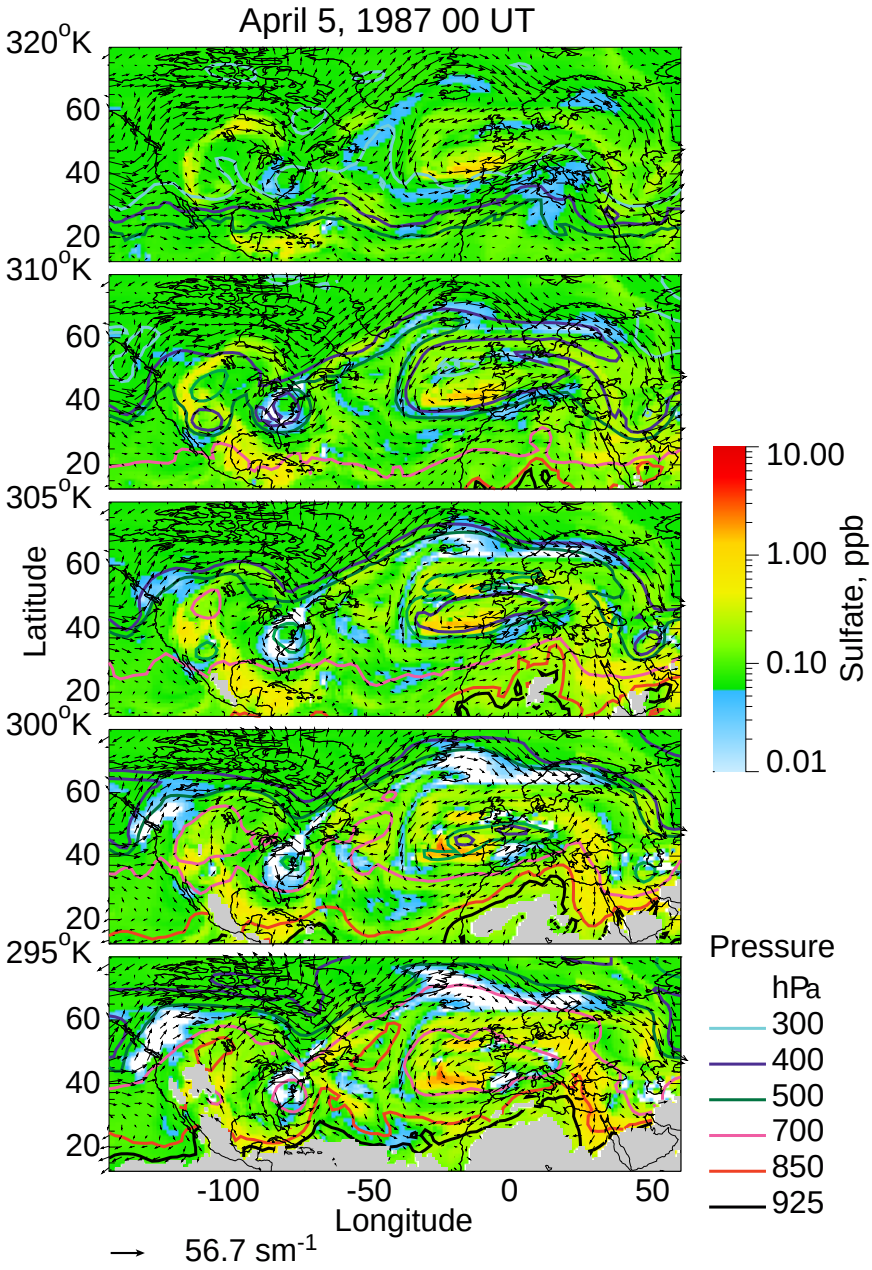

Figure 7. Isentropic analysis for 5 April 0000 UT. As in Figure 4.

contours close together in the synoptic animation for this date) and extended from northern Poland across Ireland and into the Atlantic. Because the air had originated over cold, dry land in this region the slower gas-phase conversion predominated (Figure 9) and the sulfate column burden was not large. Once over the Atlantic the cutoff low started picking up moisture, and the SO_2 column burden decreased as the circulation turned south around

the core of the system. The region of large sulfate column burden was located predominantly where the system picked up moisture: over the ocean along the southern border of the low and in the core (where in addition the pressure gradients were shallow); aqueous-phase conversion predominated in both these regions (Figure 9). The sulfate column burden in the region of the cutoff low north of ~38°N is derived predominantly from European sources (Figure 10); North American sources were the main contributors south of this latitude. As the cutoff low grew, on April 6 0600 UT (Figure 8) the regions of large sulfate and SO_2 column burden extended farther south into the Atlantic. Large sulfate column burdens extended down to ~36°N over the Atlantic, and from France east to 30°E, except for a small band off the western coast of the Iberian Peninsula where precipitation had depleted the sulfate (see corresponding panel in Animation 4). The sulfate burden over the European continent increased because the cutoff low was recirculating the sulfate generated over the ocean back over Europe; the region where aqueous-phase conversion predominated (Figure 9) extended all along the southern border of the cutoff low east to 30°E and European sources dominated all regions of large sulfate column burden (Figure 10). The effects of this low are also illustrated in the time series of the contribution of each source region to the total amount (volume integral of the sulfate concentration) presented in Figure 11, which shows an increase in the contribution of sulfate from European sources in longitude bands C and D.

[41] We now examine the influence of the eastern Atlantic cutoff low at a specific location situated southwest of the Iberian Peninsula, 22.5°W, 37.5°N (denoted by the black circles in Figures 8–10), well removed from the sulfur source areas of Europe and North America. Note in Animation 3 that from March 31 0000 UT to April 2 0000 UT this area came increasingly under the influence of a large-magnitude plume from North America. By April 5 0000 UT some of that material still remained, but it was being encroached upon by the material from the European continent under the influence of the cutoff low.

[42] On April 5 0600 UT both the sulfate and the SO_2 column burden at this location were low, with a sulfate fraction of ~0.7 (Figure 8). On this date, ~87% of the sulfate column burden was generated by aqueous-phase conversion (Figure 9), and <1% by primary emissions, with ~65% of the burden contributed by North American sources (Figure 10). After the material transported by the cutoff low reached this location, on April 6 0600 UT, the total sulfur column burden rose by an order of magnitude, but the sulfate fraction dropped to ~0.5; ~61% of the sulfate column burden was generated by aqueous-phase conversion and ~10% by primary emissions, with ~84% of the burden contributed by European sources.

[43] The time evolution of the vertical profiles of the sulfate and SO_2 concentrations (Figure 12) shows large increases in sulfate concentration from April 5 1200 UT to April 6 0000 UT and in SO_2 concentration below 2 km starting 6 hours later. These increases are due mainly to increases from European sources at low altitudes as material in the cutoff low reached the study location. On April 5 0600 UT the SO_2 concentrations were largest at an altitude of ~4 km and were dominated by North American sources; these emissions had undergone slantwise ascent on the western margin of the Atlantic, traveled across north of Labrador, and had undergone slantwise descent before arriving at this location, as indicated in the isentropic analysis for April 4 0000 UT and April 5 0000 UT (Figures 6 and 7). Because of this long-range transport and ascent the contribution from North American sources extends

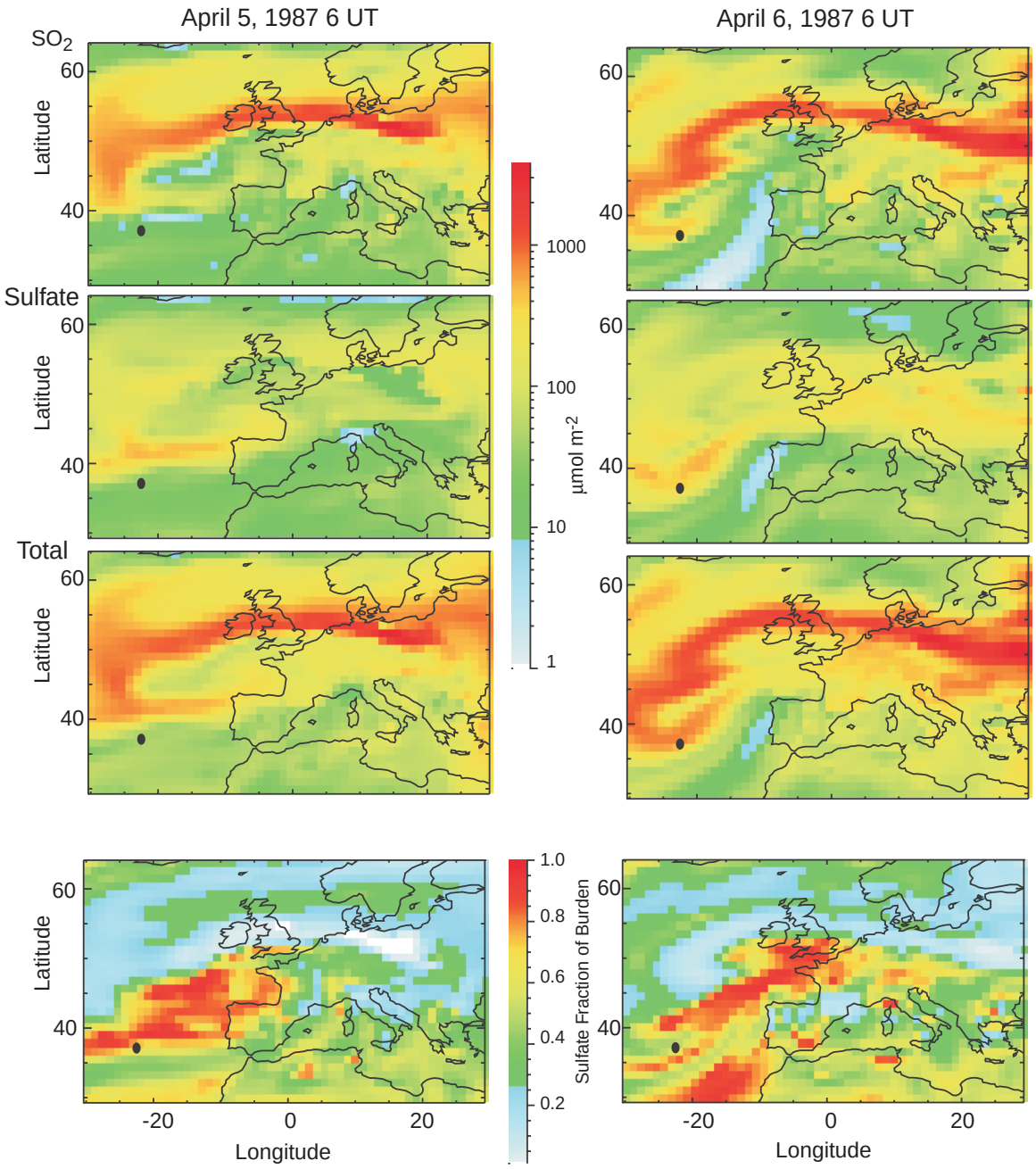

Figure 8. Sulfur (SO_2 + sulfate) column burden on April 5, 1987, 0600 UT and April 6, 1987, 0600 UT. From top to bottom: SO_2 column burden, sulfate column burden, total sulfur column burden, and sulfate fraction of the total column burden. Black symbols denote location of site (22.5°W, 37.5°N) chosen for detailed analysis of sources and formation mechanisms of sulfur species.

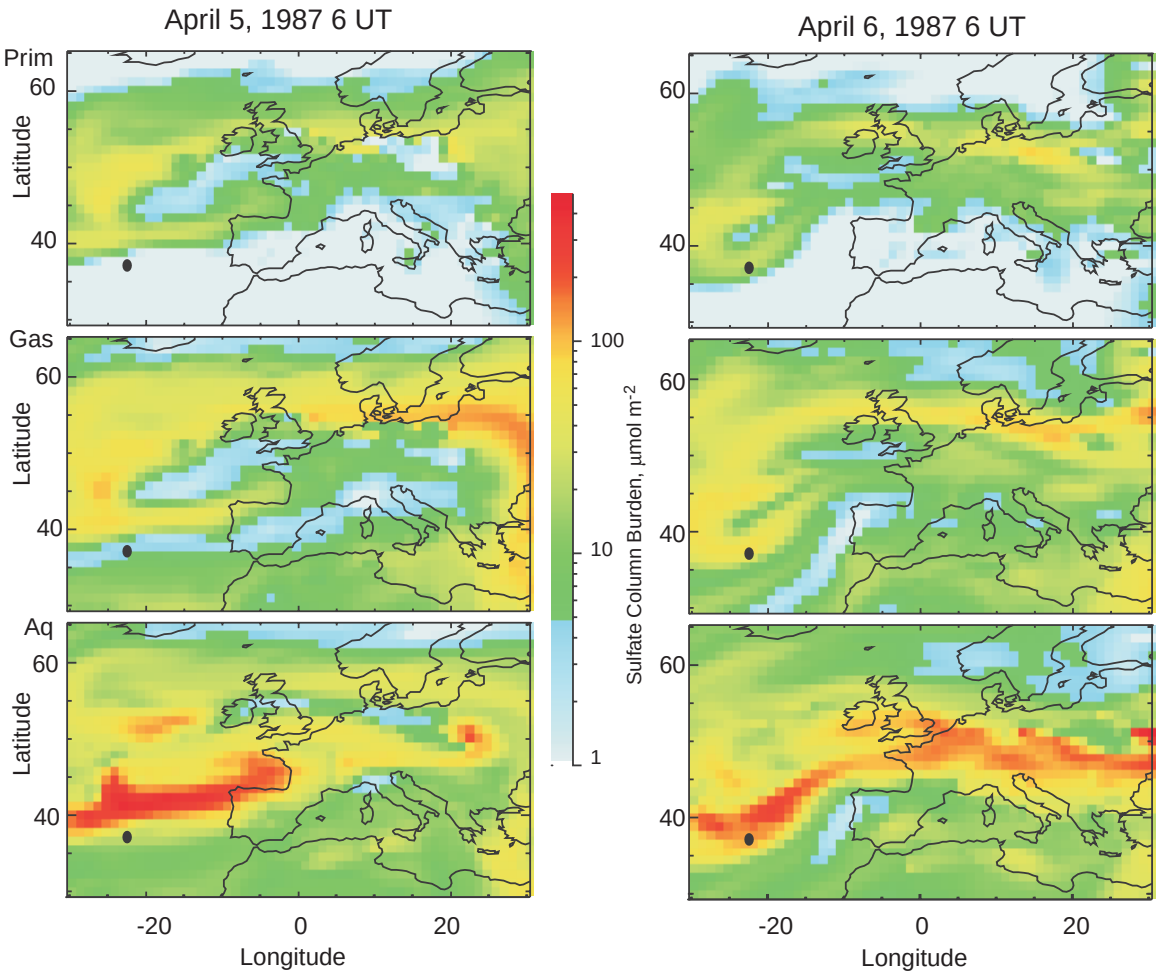

Figure 9. Sulfate column burden on April 5, 1987, 0600 UT and April 6, 1987, 0600 UT. From top to bottom: primary, secondary by gas-phase formation, and secondary from aqueous-phase conversion. Black symbols denote location of site (22.5°W, 37.5°N) chosen for detailed analysis of sources and formation of sulfur species.

up to ~10 km; because the source regions are closer, concentration from European sources was important only up to 5 km.

[44] On April 5 1200 UT, when transport of material from Europe under the influence of the cutoff low had started to affect the study location, the concentration of SO_2 was still largest at ~4 km, and North American sources still predominated at this altitude, but the contribution from European sources was starting to increase at ~1 km. The concentration of sulfate was still largest at the surface, but the contribution from European sources had increased while the contribution of North American sources remained about the same. The predominant formation process for sulfate at all altitudes was still aqueous-phase oxidation.

[45] Associated with the passage of a surface cold front at this location on April 5 1800 UT, the vertical profiles of SO_2 dramatically

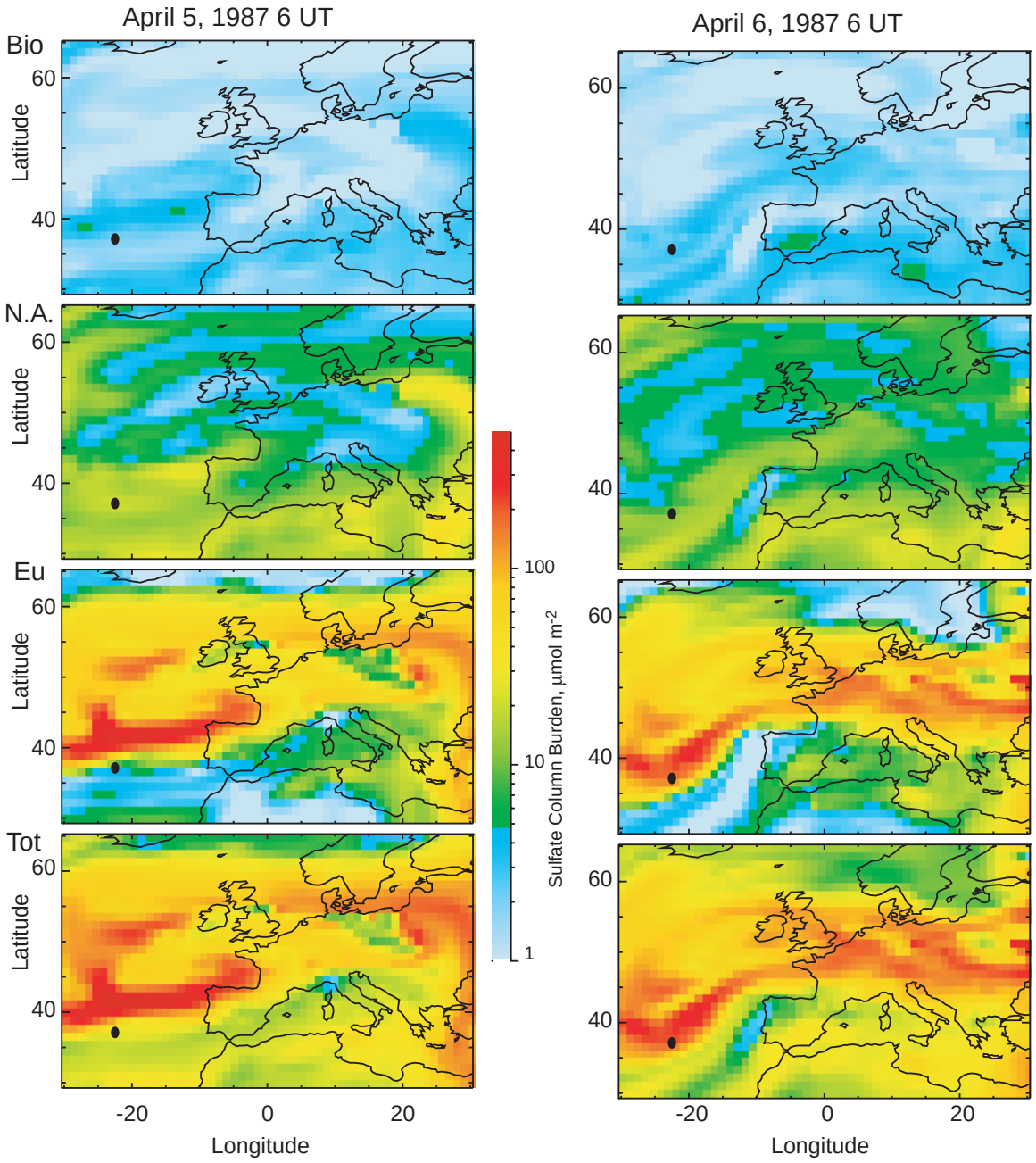

Figure 10. Sulfate column burden on April 5, 1987, 0600 UT and April 6, 1987, 0600 UT. From top to bottom: derived from biogenic sources, derived from North American sources, derived from European sources, and derived from all sources in the model domain. Black symbols denote location of site (22.5°W, 37.5°N) chosen for detailed analysis of sources and formation mechanisms of sulfur species.

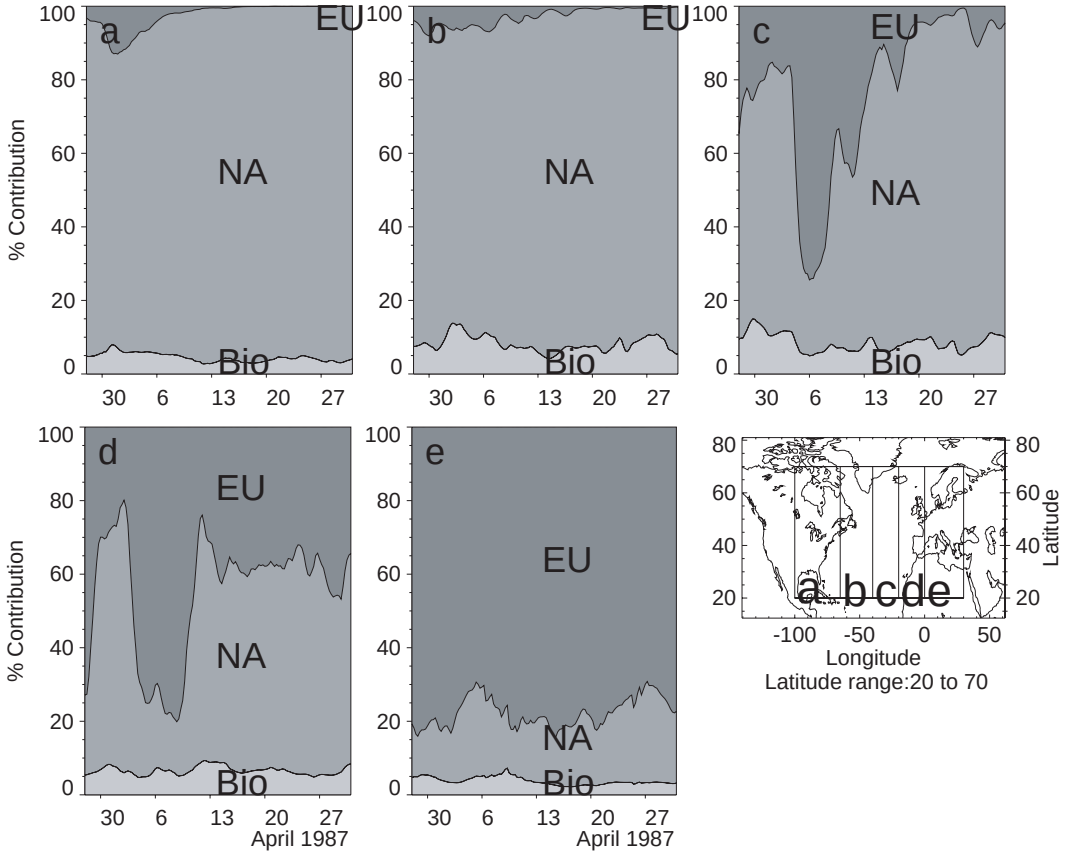

Figure 11. Time series of the percent contribution from each formation mechanism to the sulfate burden in five longitude bands: (a) 100°W to 65°W, (b) 65°W to 40°W, (c) 40°W to 20°W, (d) 20°W to 0°, and (e) 0° to 30°E. NA refers to anthropogenic sources west of 30°W, Eu refers to anthropogenic sources east of 30°W; Bio refers to biogenic sources.

changed. Evidence of this front is seen in the 500 and 925 hPa analyzes as a narrow trough that extends to the southwest of the surface and upper level lows. After the leading edge of the cold front passed over the study location, there was subsidence in the cold air mass, creating an inversion that capped the boundary layer. Following the height contours at 925 hPa on April 5 1800 UT shows that parcels at the study location originated over continental sources but were unable to mix vertically owing to the subsidence inversion in the cold air mass in which the SO_2 was released; this lack of ascent is also seen in the 295%K isentropic surface in Figure 7 (wind vectors do not cross over isobars). This atmospheric vertical structure resulted in concentrations of SO_2 more than double those at previous times, with the contribution from European sources predominating; because of the inversion present the peak concentrations were low, ~1 km. As the cutoff low stalled off the European continent, both the sulfate and SO_2 concentrations continued to increase, but the contribution from North American sources became very small at all vertical levels. As the material in the cutoff low was recirculated over Europe, more emissions were added, and by April 6 0600 UT,

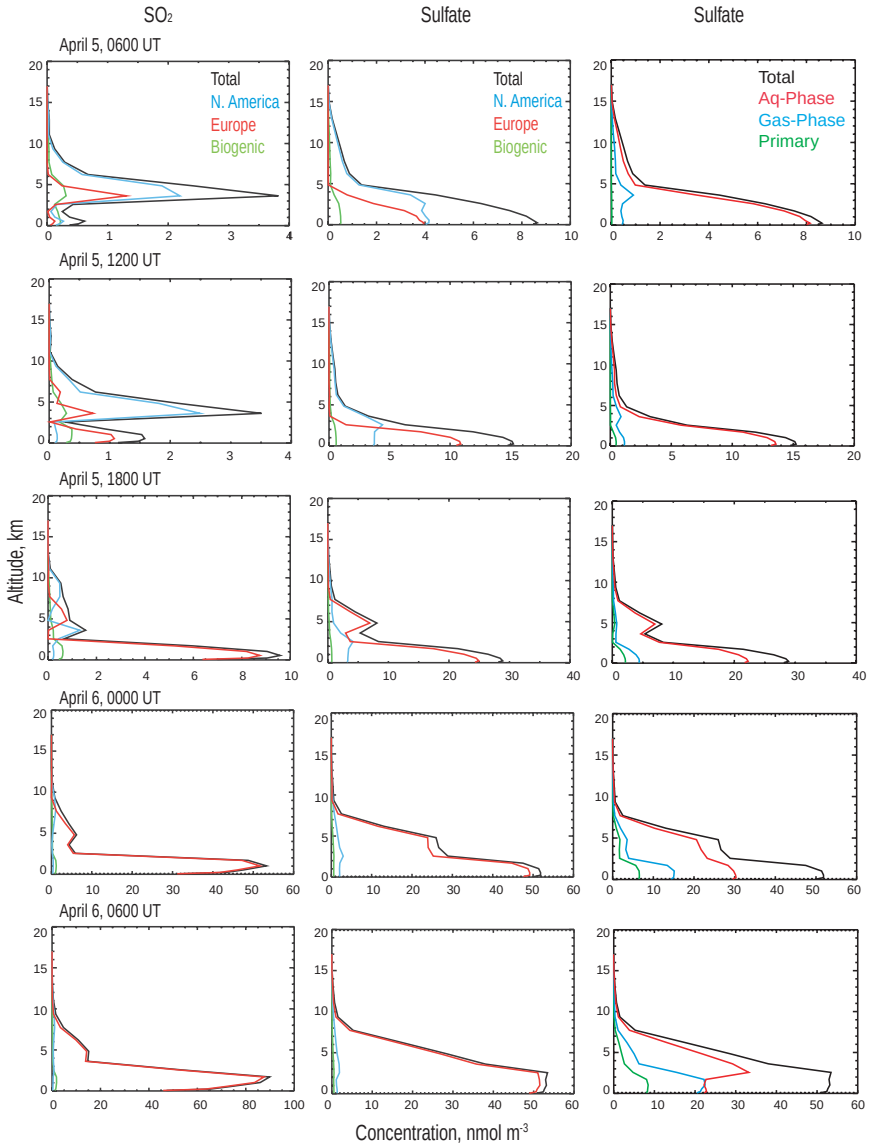

Figure 12. Vertical profiles of (left) SO_2 and (middle) sulfate concentrations derived from emissions in different source regions, and vertical profiles of (right) sulfate concentrations resulting from different formation processes for April 5, 1987, 0600 UT to April 6, 1987, 0600 UT at location 22.5°W, 37.5°N. Note increase in abscissa range for each panel.

primary emissions and gas-phase oxidation became important below 2 km.

[46] The sulfate and SO_2 were probably entrained into the low-level circulation in the vicinity of the United Kingdom, northeast of the center of low pressure. This material was circulated around the low eventually arriving at the occluded front on west-southwest winds south of the low, with the result that sulfur loading from European sources rapidly overwhelmed that from North American sources at the study location.

6. Summary and Conclusions

[47] While it has been recognized for some time that loadings of trace constituents such as sulfate and SO_2 are highly variable in space and time as a consequence of the variation in the meteorological synoptic conditions responsible for production, transport, and removal of these short-lived species, it has not been readily possible to display this variation and therefore to relate it to the combined workings of geographic distributions of sources, atmospheric chemistry, and meteorology that drive this variability. Here we have taken advantage of newly available technology of computer animation of model output and synoptic analysis together with electronic publication to present results of model calculations that display this variability. Animations of synoptic analysis were used to elucidate the interactions among several governing processes that are responsible for the transport of material over large distances as well as conditions that can give rise to large column burdens of these materials.

[48] The animations show several instances in which sulfate builds up over a several day period of anticyclonic circulation, and several instances of cutoff low-pressure systems some of which generated small column burdens, whereas others generated large column burdens; the different behavior of the cutoff lows is a consequence of their location relative to sources of sulfur and moisture. The animations have facilitated examination of an instance extending over several days in which sulfate from European sources resulted in substantial column burden over the eastern North Atlantic as far west as Iceland under the influence of a well-defined cutoff low pressure system. The circulation of material is readily seen in the animations, which show large concentrations of sulfate and SO_2 in various areas of the cutoff low, with narrow bands within the storm containing extreme concentrations (Figures 8–10). These bands occur as the tight, concentric pressure gradients associated with cutoff lows and recirculate the same air parcels over SO_2 sources. It is anticipated that such cases may provide an opportunity to examine influence of anthropogenic aerosols on cloud microphysical properties.

[49] This study reinforces the role of anticyclones in sulfate and SO_2 accumulation over large regions and adds cutoff lows as another synoptic situation that can result in the accumulation of these species. The climatology of these two synoptic systems is quite different because the peak frequency of large, slow-moving anticyclones is in the autumn in mid-latitudes, whereas the peak frequency of cutoff lows is in the spring. Given that the neither type of synoptic system is dominant in the winter and summer, the implication is that the weather patterns of the transition seasons can result in large sulfur concentrations. These results complement those of *Berkowitz et al.* [1996], who identified cyclonic systems as the main synoptic-scale mechanism responsible for transport of ozone from urban areas in North America to the western Atlantic during the summer.

[50] The ability to prepare animations may facilitate examination of such issues as the influence of exogenous materials on a given site of interest. This has immediate implications in air quality management, as it is clear that no local solution will suffice to meet air quality standards if much of the material is of exogenous origin. To facilitate tracking of the exogenous contribution we have tagged material by region of origin. It is found in certain instances that North American sulfate can dominate the column burden and concentration even in the eastern North Atlantic.

7. Implications

[51] Anticyclonic circulations that coincide with blocking ridges in the upper atmosphere can produce widespread stagnation over a period of up to a couple of weeks. These blocks often recur over the same location during a given season and may provide conditions through which the forcing mechanisms and consequences associated with sulfate accumulation may be extended to climatological timescales. These consequences include radiative forcing by sulfate aerosol and long-term air quality. For example, because cloud-free skies are common in blocking anticyclones, the direct effect of sulfate aerosol on global albedo is most pronounced in these regions, and consequently the magnitude of the direct effect varies from season to season, depending on the frequency and geographic location of significant blocking features.

[52] Cutoff lows that have developing stages with ready access to moisture act as sinks for sulfate; those that form over continental areas away from moisture sources act as sulfate accumulators. Thus cutoff lows commonly observed along the East Coast of the United States and along the east coast of China and the former Soviet Union are more likely to act as sulfate sinks than accumulators because of their locations during the developing stages are close to sources of moisture. Similarly, cutoff lows along the West Coast of the United States, the west coast of Europe, and over continental areas removed from moisture sources are more likely to act as sulfate accumulators. Certain global weather patterns that modulate the frequency and location of cutoff lows can significantly impact the amount of sulfate present in the atmosphere at a given time, either by enhancing the cutoff lows that accumulate sulfate or the systems that wash out sulfate. This in turn has important implications in air quality, acid rain, and radiative transfer.

Appendix A: Glossary of Terms

Advection: the horizontal movement of a mass of fluid; also transport by such movement.

Ageostrophic flow: under *geostrophic flow* the *Coriolis force* and *pressure gradient* forces are balanced, thus producing flow parallel to the height *isolines*. If another force is present besides the Coriolis and pressure gradient forces, a parcel will not travel parallel to isolines of height on a constant pressure surface but will have a component across the isolines of height. Additional forces that are associated with ageostrophic flow are friction (near the surface) and centrifugal force (in curved flow). Horizontal convergence and divergence in the flow, which are necessary to produce vertical motion, are possible only if the flow is ageostrophic.

Anticyclone: a system of winds that rotates about a center of high atmospheric pressure, clockwise in the Northern Hemisphere, with a typical diameter of 2400–4000 km and which usually advances at 30 to 50 km h^{-1}.

Aqueous-phase oxidation: here, the oxidation of SO_2 to sulfate in cloud liquid water by hydrogen peroxide (H_2O_2) and to a lesser extent by ozone (O_3).

Baroclinic leaf: an elongated, synoptic cloud feature on satellite photos that denotes the area of saturated slantwise ascent on an isentropic analysis. A baroclinic leaf is often associated with a warm conveyor belt of a developing cyclone and typically has a sharp cloud edge on its western boundary.

Blocking pattern: A synoptic pattern characterized by little or no temporal progression of synoptic features. Blocking patterns are robust features of the upper level flow that tend to recur during a particular season over a given geographic location; climatological features such as El Niño often modulate the upper level flow to favor a particular hemispheric weather pattern, thereby inducing the recurrence of these blocks over specific areas.

Blocking ridge: the development of a warm ridge or cutoff high aloft at high latitudes that becomes associated with a cold high at the surface, causing a split in the westerly winds. Such a high will move very slowly, tending to move westward during intensification and eastward during dissipation. It prevents the movement of migratory cyclones across its latitudes. Two examples are a cutoff high and an *omega block*.

Column burden: the vertical integral of the concentration of an atmospheric trace species at each vertical level.

Concentration: the amount of a chemical species in a given volume; cf. *mixing ratio*.

Confluence: a pattern of wind flow in which air flows inward toward an axis oriented parallel to the general direction of flow. It is the opposite of difluence. Confluence is not the same as convergence. Winds often accelerate as they enter a confluent zone, resulting in speed divergence that offsets the (apparent) converging effect of the confluent flow [*Glickman*, 2000].

Constant pressure analysis: An analysis performed at a specified pressure in the atmosphere. A 500 hPa analysis refers to the analysis of a variable at a pressure level of 500 hPa.

Cutoff low pressure system: a cluster of *isolines* of *sea level height* on a constant pressure surface above ~700 hPa (usually 500 hPa) that form concentric near circles of decreasing radius with the smallest circle representing the lowest sea level height; a minimum in the sea level height with relatively uniform upward slope toward greater heights in all directions. These clusters are "cut off" from the main axis of the jet stream and contain only a small zonal flow component to the jet stream axis or to translating wave disturbances. Hence they are slow-moving features of the synoptic flow pattern and can persist for several days with little or no translation. The development of a cutoff low aloft is typically associated with strong surface development (formation of a deep minimum in surface pressure) and represents the occlusion, or decaying stage, of a mature midlatitude cyclone. Cutoff lows can be observed during any season but are most frequent in the transition seasons, spring and autumn.

Cyclogenesis: a process whereby a cyclone develops where none previously existed owing to a combination of upper level and surface features.

Entropy: a mathematically defined thermodynamic function of state, the increase in which gives a measure of the energy of a system that has ceased to become available for work during a certain process.

Equivalent potential temperature: the *potential temperature* that a parcel of air would have if all its moisture were condensed out and the resultant latent heat used to warm the parcel.

Eta (η) coordinates: the eta coordinate varies linearly with pressure from zero at the top of the model domain (typically 50 mbar) to unity at the mean sea level pressure. As a result of being related to the sea level pressure, the eta coordinate system does not produce significant sloping of the eta surfaces over steeply sloping terrain. The vertical levels are spaced with the thinnest layers near the surface [*Black*, 1994].

Gas-phase oxidation: here, the oxidation of SO_2 to sulfate via the reaction with the hydroxyl radical (OH) in the gas phase.

Geostrophic flow: in the upper atmosphere the coriolis and pressure gradient forces on a given parcel in straight flow are balanced; this causes the flow to be parallel to isolines of height on a constant pressure surface; cf. *ageostrophic flow*.

Gradient transport assumption: turbulent flux of a species can be approximated by (minus) the product of an eddy diffusivity tensor (which is generally assumed to be diagonal) times the gradient of the species' mixing ratio. This assumption (and the turbulent flux approximation) is also referred to by "first-order closure" and "K theory." An important property of this assumption is that the turbulent flux is always downgradient, moving material from a region of

higher mixing ratio to one of lower mixing ratio [*Hales*, 1989].

Hydrostatic: the hydrostatic approximation implies that the pressure at any height in the atmosphere is equal to the weight of the atmosphere above that height. This approximation can be used only when vertical motions in the atmosphere (such as convection) are negligible.

Isentropic analysis: surfaces of constant potential temperature are also surfaces of constant *entropy*, hence the name isentropic. It is possible to use the *equivalent potential temperature* of a parcel as an indication of its vertical position in the *troposphere*. An advantage of isentropic coordinates is that parcels in motion remain on the same isentrope as they move over long distances. Therefore, to trace the three-dimensional trajectory of a parcel, the pressure and wind vector are plotted on an isentropic surface (a surface with constant potential temperature). If the wind vector indicates that parcels on the isentropic surface are being transported toward higher pressures, they must be moving toward the ground as they are transported horizontally. The likelihood of a given region to experience *slantwise* motions is therefore directly proportional to the gradient of pressure and the wind speed and direction on an isentropic surface. If the wind direction is parallel to the isobars on an isentropic surface, slantwise ascent or descent is not indicated. One limitation of isentropic analysis is that isentropic surfaces may intersect the ground in tropics and in mountainous areas.

Isentropic surfaces: surfaces of constant *entropy* (and also of constant *equivalent potential temperature*).

Isolines: contours along which the value of a scale is constant. The prefix "iso" is often affixed to a variable to indicate a contour of that variable, e.g., isobar that signifies lines of equal barometric pressure.

Jet stream: relatively strong winds concentrated within a narrow stream in the atmosphere. While this term can be applied to any atmospheric flow including the vertical component, it is usually used to refer to the quasi-horizontal jet stream of winds associated with the midlatitude westerlies. This band of winds is concentrated in the high troposphere.

Meridional flow, meridional meander: large-scale atmospheric flow in which the north-south component (i.e., longitudinal, or along a meridian) is pronounced. The accompanying zonal (east-west) component often is weaker than normal [*Glickman*, 2000].

Mixing ratio: amount of an atmospheric trace species (mol) per mole of air 1 nmol/mol (air) = 1 part per billion, ppb. Mixing ratio is useful to express atmospheric abundance because it is unchanged when an air parcel expands or contracts because of changes in pressure and temperature, cf. *concentration*.

Omega (Ω) blocking pattern: an extremely stable upper air flow configuration that is shaped like the Greek letter omega. Such features may last for days or weeks blocking the natural west-to-east progression of weather systems and material transport.

Optical depth: a measure of the turbidity of the atmosphere in the visible and near-infrared wavelengths; the negative logarithm of the direct beam transmittance through a vertical column.

Potential temperature: the temperature a parcel of unsaturated air would have if brought adiabatically from its initial state to an arbitrarily selected pressure of 1000 hPa.

Primary: material emitted directly into the atmosphere (as opposed to secondary).

Radiosonde: the instrument package attached to a weather balloon that records the pressure, temperature, and relative humidity as a function of the three-dimensional position of the package. This information is transmitted back to the launch site and allows the calculation of the wind vector as a function of height.

Ridge: a relative maximum in the pressure field or height field on a constant pressure

surface that is not characterized by closed contours. A ridge can be identified on upper air charts as a location at which heights bulge to the north (in the Northern Hemisphere) on a constant-pressure surface. A ridge is often part of a system that resembles a sinusoidal wave in the jet stream and will possess a "ridge axis" in which the synoptic flow to the east will have a northerly component and the flow to the west will have a southerly component. Ridges in certain configurations can represent "blocks" in the flow, particularly when they resemble a Greek letter omega (Ω), and can persist at the same locations for more than a week and up to two to three weeks in extreme situations; see *Omega block*.

Sea level pressure: pressure measurements in the atmosphere are conventionally adjusted to a universal datum, sea level. This allows the construction of isobaric charts in complex terrain where, otherwise, a surface isobaric chart would simply be a map of the height of the terrain.

Secondary: material formed in the atmosphere from emissions of precursor species (as opposed to *primary*).

Stagnant weather pattern (or stagnation): a weather pattern that is not advancing or developing.

Slantwise: pertaining to a widespread slow ascent or descent on the synoptic scale (1000 km). In the isentropic analysis figures, slantwise ascent/descent is present whenever wind vectors cross pressure contours.

Surface low: a minimum in the sea level barometric pressure characterized by a counterclockwise, inward spiraling horizontal wind field.

Synoptic flow: wind flow over large areas (around 1000 km^2) is governed by the synoptic distribution of pressure or height on a constant pressure surface. Local pressure perturbations are not considered as elements of the synoptic flow, only regional pressure gradients are relevant.

Synoptic scale: a system having a distance scale of the order of 1000 km and a timescale on the order of days.

Troposphere: the lowest 8–12 km of the atmosphere. It is the layer within which all observable weather impacting the surface on a daily basis is observed.

Trough: a relative minimum in the pressure field or height field on a constant pressure surface that is not characterized by closed contours. A trough is often described as an "open wave" and can be identified on upper air charts as a location of a constant pressure surface where low heights to the north "sag" to the south (Northern Hemisphere). A well-developed trough will be part of a system that resembles a sinusoidal wave in the jet stream and will possess a "trough" axis in which the synoptic flow to the east will have a southerly component and the flow to the west will have a northerly component. See *ridge*.

Uninitialized analysis: meteorological variables as predicted by forecast models before observations are merged with the model output to adjust results by four-dimensional (position, time) data assimilation.

Warm conveyor belt: a synoptic system precipitating over a wide area, not necessarily associated with a well-organized *surface low*. A *baroclinic leaf* often appears in conjunction with a warm conveyor belt as an elongated cloudy region stretching through tens of degrees latitude from tropical regions into the midlatitudes. Baroclinic leafs act as conveyor belts by collecting moist parcels from the tropics and moving them gradually higher in the atmosphere with increasing latitude, typically transporting parcels from southwest to northeast along the trajectory. A baroclinic leaf associated with an approaching upper level trough, perhaps being associated with a stationary or weak cold front, may eventually become part of the circulation of a mature cyclone, leading to a distortion of the cloud system in response to a developing circula-

tion and the development of a complex system of additional transport conveyor belts.

Wind conventions: in meteorology, "the wind is named from where it came," so a southwesterly wind blows from southwest to northeast.

Zonal flow: geophysical fluid flow parallel to latitude lines. A completely zonal flow is indicated by isolines of sea level height on a constant pressure surface above ~700 hPa. A flow that is dominated by its zonal component is often characterized by rapidly translating weak disturbances (slight meridional meanders) moving from west to east, which causes the weather in a given area to change frequently. Disturbances associated with zonal flows are weak and short-lived and modified maritime air masses tend to dominate continental areas during zonal periods. See *meridional flow.*

Acknowledgments

[53] The meteorological data used were supplied by the European Centre for Medium-Range Weather Forecasts (ECMWF). We thank Song-you Hong (NCEP and Yonsei University, Seoul, Korea) for assistance with the NCEP reanalysis data and Seth Nemesure (BNL), who developed the methodology used to create the sulfur animations. The work of C.M. Benkovitz and S.E. Schwartz was supported by the Environmental Sciences Division of the U.S. Department of Energy as part of the Atmospheric Chemistry Program and was performed under contract DE-AC2-98CH10886. The work of M.A. Miller was funded by the National Aeronautics and Space Administration (NASA) Sensor Intercomparison and Merger for Biological Interdisciplinary Ocean Studies (SIMBIOS), contract #52-210.91. The work of O-Ung Kwon at BNL was supported by the Korea Meteorological Administration.

References

Bates, T. S., B. K. Lamb, A. Guenther, J. Dignon, and R. E. Stoiber, Sulfur emissions to the atmosphere from natural sources, *J. Atmos. Chem.*, *14*, 315–337, 1992.

Benkovitz, C. M., and S. E. Schwartz, Evaluation of modeled sulfate and SO_2 over North America and Europe for four seasonal months in 1986–87, *J. Geophys. Res.*, *102*, 25,305–25,338, 1997.

Benkovitz, C. M., C. M. Benkowitz, R. C. Easter, S. Nemesure, R. Wagener, and S. E. Schwartz, Sulfate over the North Atlantic and adjacent continental regions: Evaluation for October and November, 1986 using a three-dimensional model driven by observation-derived meteorology, *J. Geophys. Res.*, *99*, 20,725–20,756, 1994.

Benkovitz, C. M., M. T. Scholtz, J. Pacyna, L. Tarrasón, J. Dignon, E. V. Voldner, P. A. Spiro, J. A. Logan, and T. E. Graedel, Global gridded inventories of anthropogenic emissions of sulfur and nitrogen, *J. Geophys. Res.*, *101*, 29,239–29,253, 1996.

Berkowitz, C. M., P. H. Daum, C. W. Spicer, and K. M. Busness, Synoptic patterns associated with the flux of excess ozone to the western North Atlantic, *J. Geophys. Res.*, *101*, 28,923–28,933, 1996.

Black, T. L., The new NMC mesoscale eta model: Description and forecast examples, *Weather Forecast.*, *9*, 265–278, 1994.

Bott, A., A positive definite advection scheme obtained by nonlinear renormalization of the advective fluxes, *Mon. Weather Rev.*, *117*, 1006–1015, 1989.

Charlson, R. J., J. Langner, H. Rodhe, C. B. Leovy, and S. G. Warren, Perturbation of the Northern Hemisphere radiative balance by backscattering from anthropogenic aerosols, *Tellus*, *43*, 152–163, 1991.

Charlson, R., S. E. Schwartz, J. M. Hales, R. D. Cess, J. J. A. Coakley, J. E. Hansen, and D. J. Hoffman, Climate forcing by anthropogenic aerosols, *Science*, *255*, 423–430, 1992.

Easter, R. C., Two modified Versions of Bott's Positive Definite Numerical Advection Scheme, *Mon. Weather Rev.*, *121*, 297–304, 1993.

European Centre for Medium-Weather Forecasting (ECMWF), *User Guide to ECMWF Products* version 1.1, Eur. Cent. for Medium-Range Weather Forecasts, Reading, England, 1988.

ECMWF Research Department, *Research Manual 3 ECMWF Forecast Model: Physical Parametrization*, Eur. Cent. for Medium-Range Weather Forecasts, Reading, England, 1991.

Glickman T. S. (Ed.), *Glossary of Meteorology*, 2nd ed., 855 pp., Am. Meteorol. Soc., Boston, Mass., 2000.

Hales, J. M., A generalized multidimensional model for precipitation scavenging and atmospheric chemistry, *Atmos. Environ.*, *23*, 2017–2032, 1989.

Haywood, J. M., V. Ramaswamy, and B. J. Soden, Tropospheric aerosol climate forcing in clear-sky satellite observations over the oceans, *Science*, *283*, 1299–1303, 1999.

Husain, L., and V. A. Dutkiewicz, A long-term (1975–1988) study of atmospheric SO_4^{2-}: Regional contribu-

tions and concentration trends, *Atmos. Environ., Part A*, *24*, 1175–1187, 1990.

Husar, R. B., and W. E. Wilson, Haze and sulfur emission trends in the eastern United States, *Environ. Sci. Technol.*, *27*, 12–16, 1993.

Husar, R. B., J. M. Prospero, and L. L. Stowe, Characterization of tropospheric aerosols over the oceans with the NOAA Advanced Very High Resolution Radiometer Optical Thickness Operational Product, *J. Geophys. Res.*, *102*, 16,889–16,909, 1997.

Kalnay, E., M. Kanamitsu, R. Kistler, W. Collins, D. Deaven, L. Gandin, M. Iredell, S. Saha, G. White, J. Woollen, Y. Zhu, M. Chelliah, W. Ebisuzaki, W. Higgins, J. Janowiak, K. C. Mo, C. Ropelewski, J. Wang, A. Leetmaa, R. Reynolds, R. Jenne, and D. Joseph, The NCEP/NCAR 40-Year Reanalysis Project, *Bull. Am. Meteorol. Soc.*, *77*(3), 437–471, 1996.

Kentarchos, A. S., and T. D. Davies, A climatology of cut-off lows at 200 hPa in the Northern Hemisphere, 1990–1994, *Int. J. Climatol.*, *18*, 379–390, 1998.

Kiehl, J. T., and B. P. Briegleb, The relative roles of sulfate aerosols and greenhouse gases in climate forcing, *Science*, *260*, 311–314, 1993.

Kiehl, J. T., T. L. Schneider, P. J. Rasch, M. C. Barth, and J. Wong, Radiative forcing due to sulfate aerosols from simulations with the NCAR Community Climate Model (CCM3), *J. Geophys. Res.*, *105*, 1441–1458, 2000.

Lyons, W. A., Evidence of transport of hazy air masses from satellite imagery, *Ann. N. Y. Acad. Sci.*, *338*, 418–433, 1980.

Mitchell, J. F. B., T. C. Johns, J. M. Gregory, and S. F. B. Tett, Climate response to increasing greenhouse gases and sulphate aerosols, *Nature*, *376*, 501–504, 1995.

Namais, J., Forecasting significance of anticyclonic eddies on isentropic surfaces, *Eos Trans. AGU*, 1938.

Namais, J., The use of isentropic analysis in short term forecasting, *J. Aeronaut. Sci.*, *6*(7), 1939.

Parker, S. S., J. T. Hawes, S. J. Colucci, and B. P. Hayden, Climatology of 500 mb cyclones and anticyclones, 1950–85, *Mon. Weather Rev.*, *117*, 558–570, 1989.

Schimel, D., D. Alves, I. Enting, M. Heimann, F. Joos, D. Raynaud, T. Wigley, M. Prather, R. Derwent, D. Ehhalt, P. Fraser, E. Sanhueza, X. Zhou, P. Jonas, R. Charlson, H. Rodhe, S. Sadasivan, K. P. Shine, Y. Fouquart, V. Ramaswany, S. Solomon, J. Srinivasan, D. Albritton, R. Derwent, I. Isaksen, M. Lal, and D. Wuebbles, Radiative forcing of climate change in *Climate Change 1995. The Science of Climate Change*, edited by J. A. Lakeman, 65–132, Cambridge Univ. Press, New York, 1996.

Schwartz, S. E., and A. Slingo, Enhanced shortwave cloud radiative forcing due to anthropogenic aerosols in *NATO ASI Series: Clouds, Chemistry and Climate*, edited by P. J. Crutzen and V. Ramanathan, 191–236, Springer-Verlag, New York, 1996.

Seinfeld, J. H., and S. N. Pandis, *Atmospheric Chemistry and Physics*, 1326 pp., John Wiley, New York, 1998.

Simmons, A. J., and R. Struffing, *An Energy and Angular-Momentum Conserving Finite Difference Scheme, Hybrid Coordinates and Medium-Range Weather Prediction*, Eur. Cent. for Medium-Range Weather Forecasts, Reading, England, 1981.

Spivakovsky, C. M., R. Yevich, J. A. Logan, S. C. Wofsy, M. B. McElroy, and M. J. Prather, Tropospheric OH in a three-dimensional chemical tracer model: An assessment based on observations of CH_3CCl_3, *J. Geophys. Res.*, *95*, 18,441–18,471, 1990.

Wesely, M., Simplified techniques to study components of solar radiation under haze and clouds, *J. Appl. Meteorol.*, *21*, 373–383, 1982.

Wesely, M., Parameterization of surface resistances to gaseous dry deposition in regional-scale numerical models, *Atmos. Environ.*, *23*, 1293–1304, 1989.

Yanenko, N. N., *The Method of Fractional Steps*, Springer, New York 1971.